Physics – Uspekhi **56** (1) 29 – 48 (2013)

REVIEWS OF TOPICAL PROBLEMS PACS numbers: 61.44.Fw, **62.25.–g**, 71.45.Lr, 72.20.Fr, 73.30.Mf, 78.70.Gq

High-frequency, 'quantum' and electromechanical effects in quasi-one-dimensional charge density wave conductors

V Ya Pokrovskii, S G Zybtsev, M V Nikitin, I G Gorlova,
V F Nasretdinova, S V Zaitsev-Zotov

DOI: 10.3367/UFNe.0183.201301b.0033

Contents

Abstract. Recent results (some previously unpublished) on the physics of charge density waves (CDWs) are reviewed. The synthesis conditions and unique properties of the quasi-one-dimensional compound NbS_3, with highly coherent room temperature CDWs, are described. A peculiar type of 'quantization' is discussed, which is observed in micro- and nanosamples of $K_{0.3}MoO_3$ and $NbSe_3$ due to the discrete nature of CDW wave vector values. The electric-field-induced torsional strain (TS) in quasi-one-dimensional conductors is considered. Research results on the TS of a noise character induced by sliding CDWs are presented, along with those on the inverse effect, the modulation of the voltage induced by externally driven TS. Results on the nonlinear conduction of TiS_3, a quasi-one-dimensional compound not belonging to the family of classical Peierls conductors, are also described.

V Ya Pokrovskii, S G Zybtsev, M V Nikitin, I G Gorlova, V F Nasretdinova, S V Zaitsev-Zotov Kotel'nikov Institute of Radioengineering and Electronics, Russian Academy of Sciences,
ul. Mokhovaya 11, korpus 7, 125009 Moscow, Russian Federation
Tel. +7 (495) 629 34 59, +7 (495) 629 36 56
Fax +7 (495) 629 36 78
E-mail: pok@cplire.ru

Received 16 December 2011, revised 18 July 2012
Uspekhi Fizicheskikh Nauk **183** (1) 33 – 54 (2013)
DOI: 10.3367/UFNr.0183.201301b.0033
Translated by Yu V Morozov; edited by A Radzig

1. Introduction

This review, based largely on the results obtained by the authors in the last 5–7 years, deals with electron transport and its relationship with the mechanical properties of quasi-one-dimensional charge density wave (CDW) conductors.

A CDW is a periodic self-consistent distortion of the crystal lattice and electron density observed at sufficiently low temperatures in metallic compounds composed of weakly bound conducting chains. There has been undiminishing interest in quasi-one-dimensional CDW conductors during the past 40 years. Although such conductors have not yet found practical application, their diverse and unique properties continue to attract the attention of researchers in different countries.

The history of CDWs dates back to Rudolf Peierls's prediction of instability of the crystal lattice in one-dimensional metals with respect to periodic distortions defined by double Fermi wave vector $2k_F$. Such distortion, known as the Peierls transition, can be described as the superposition of Fermi surfaces corresponding to k_F and $-k_F$. If the surfaces fit together perfectly, they are said to have the property of nesting. The prediction made by Peierls in the pre-war period and published in 1955 [1] was used by Fröhlich in 1954 [2] to propose a new collective mechanism of electron charge transport, and thereby to make an attempt to explain superconductivity. His explanation proved erroneous, but the proposed charge transfer mechanism was shown to actually operate 20 years later when conductors with a highly anisotropic crystalline and electronic structures were synthesized [3–7]. Reference [5] demonstrated an unusually high

conductivity in the microwave frequency range, besides nonlinear conduction, and thus gave direct evidence of the collective character of electron charge transport. Hence, although the basic ideas of the Peierls transition (confirmed by a number of experimental evidences) were formulated before 1975 [6], CDW sliding was first revealed in 1976. The main properties of CDWs are described in reviews [7, 8] and recent progress in this field is discussed in the proceedings of several workshops [9–11].

Thus, a characteristic pattern is observed in quasi-one-dimensional metals: the metal–insulator transition with lattice distortion occurring after a drop in temperature to the Peierls transition point. The period of distortion being defined by the wave vector $q = 2k_F$, a dielectric gap forms at the Fermi level, and the metal turns into a semiconductor. Then, a decrease in energy of the electron subsystem comes into play and this accounts for the observed transition. The lattice distortion is accompanied by modulation of electron density, i.e., CDW formation.

One-dimensionality, indispensable for Fermi surface nesting, is as important as interchain interaction; in other words, the conductors must be *quasi-one-dimensional*. Such interaction stabilizes phase transitions which are impossible in one-dimensional systems [12]. However, the temperature of the Peierls transition is much lower than predicted by the mean-field theory due to one-dimensional fluctuations; therefore, transition to the CDW state should rather be called three-dimensional ordering transition.

A change of CDW phase in time (sliding) results in the transfer of the charge of electrons condensed under the Peierls gap, i.e., all electrons that resided in the conduction band of the metallic state. This is just what is called the Fröhlich mode. CDW sliding is associated with the generation of narrow- and broad-band noises. The narrow-band noise frequency (also termed fundamental or washboard frequency) equals the reverse time of CDW movement by one period. It is directly proportional to the CDW velocity and may be used, in particular, to determine the charge density condensed in a CDW (if the current density is known). The fundamental frequency can also be found in experiments on CDW synchronization by an external high-frequency (HF) field (from the so-called Shapiro steps). Shapiro steps can be observed when dc bias V and alternating HF voltage are simultaneously applied to the sample [7, 8, 13]. When, at a certain value of V, the alternating voltage frequency coincides with the fundamental frequency of a sliding CDW (or one of its harmonics or subharmonics), the $I(V)$ dependence exhibits a voltage range characterized by constant CDW current, referred to as a Shapiro step. Accordingly, the dependence of $R_d \equiv dV/dI$ on V shows a peak. This effect is qualitatively explained as the action of an external HF field making a CDW creep with a given velocity in a certain voltage range (in a sense, frequency locking), due to which its differential resistance increases; it tends to infinity in the case of complete synchronization.

The infinite CDW conductivity predicted in Ref. [2] cannot be observed because of the interaction between CDWs and impurities, which enhances by virtue of the CDWs ability to deformation: the value of q changes with coordinate variation so that the CDW phase is adjusted to the impurity potential. The effect of impurities on CDWs (pinning) is characterized by coherence lengths at which phase gain is 2π due to a random phase interruption.

Pinning makes CDW sliding possible only in such electric fields, the strength of which is higher than the threshold value E_t. In strong electric fields, the CDW conductivity approximates the value that could be expected for the normal (metallic) state. Why conductivity of a CDW cannot exceed the normal conductivity of electrons condensed in it remains to be clarified. The limiting CDW creep velocity ('critical current'), whose overshoot must induce transition from the CDW state to the normal state, is not exactly known either. The experimental data suggesting that the critical current is reached and their possible interpretation are presented in Refs [14, 15], although they are not definitive. A separate problem is the limiting frequency of CDW generation or synchronization that may correspond to a current much lower than the 'critical' one.

The character of high-velocity CDW sliding is a topical issue discussed in this review because Section 2 includes the results of studies using nano-sized NbS_3 samples (phase II) with which record-breaking high CDW synchronization frequencies were obtained.

The properties of small-sized quasi-one-dimensional conductors constitute the subject matter of a special branch of CDW physics. Such samples exhibit a number of finite-size effects arising when certain dimensions of a sample become comparable to or smaller than CDW characteristic lengths. The properties of small samples were reviewed in Refs [16, 17]. One of the most interesting finite-size effects is responsible for the formation of discrete CDW states, i.e., sort of 'quantization'. If the lateral sizes of a sample are smaller than the respective coherence lengths and the sample is short enough, the creation or annihilation of even a single CDW period (~ 10 Å) may lead to experimentally observable effects. Thus, Ref. [18] reports conductivity steps in TaS_3 nanosamples related to a change in the number of CDW periods by ± 1 in single acts of CDW phase slippage. Stepwise variation of the q vector was directly observed in chromium crystals as well, where a two-dimensional spin density wave was generated [19]. We have recently observed such 'quantization' of the CDW vector in nanosamples of $K_{0.3}MoO_3$ (blue bronze) and $NbSe_3$, where CDWs proved to have a high degree of coherence. This effect is studied in Section 3.

CDW strain is closely associated with the existence of metastable states, i.e., nonequilibrium states in which CDW strain persists for a very long time. As known, metastable states in many compounds with CDWs may be created by thermal means using the temperature dependence of the wave vector. For example, a series of discrete metastable CDW states in TaS_3 or blue bronze nanosamples can be obtained at the same temperature based on their different temperature prehistories (see Section 3). Also, metastable states can be created by an electric field. The nature of such structurally nonuniform strain is fairly well known.

Apart from CDW strain, the elastic interaction between CDW, i.e., an electron crystal inside the host lattice, and the crystal itself is observed. Such interaction may be responsible for a decrease in Young's modulus if the CDW depins from impurities in the above-threshold electric fields [20]. It was later elucidated that CDW deformation results in the deformation of a crystal itself [21, 22]. Both uniform longitudinal [21] and nonuniform longitudinal [22] deformations were revealed. The accompanying effects are considered in Section 4, with special reference to torsional strain of quasi-one-dimensional CDW conductors in an electric field. The same section treats the inverse effect, i.e., voltage modulation induced by torsional strain.

Much attention has recently been attracted to compounds in which CDW generation is (possibly) unrelated to the Peierls transition, i.e., nesting [23, 24]. Interestingly, the very existence of CDWs in a such a well-known quasi-two-dimensional compound as $NbSe_2$ was questioned. The problem of a CDW nature may be just as well vital for NbS_3 (phase II) compound, where the CDW arises at $T = 150$ K and low concentration of electrons that depends in addition on the sample used (see Section 2). There are reports suggesting the existence of collective states (possibly CDWs) in the layered quasi-one-dimensional compound TiS_3, where electron concentration at room temperature is estimated to be 10^{18} cm^{-3}. If it is assumed that the lattice distortion in TiS_3 is described by usual nesting, the CDW period proves to be improbably long. The results of TiS_3 studies are considered in Section 5.

To recall, this review is not designed to comprehensively cover all research topics pertaining to quasi-one-dimensional CDW conductors, but focuses on the results recently obtained by the authors. Nevertheless, it contains a wealth of CDW physics data reported for the last 5–7 years. The study subjects included in the review are well-known compounds, such as TaS_3, $NbSe_3$, $K_{0.3}MoO_3$, $(TaSe_4)_2I$, rare NbS_3 (phase II) synthesized by the authors, and TiS_3 for which mechanisms of conductivity remain to be elucidated. Some new physical results were obtained in the course of this work, including certain formerly inaccessible values of selected parameters.

2. Synthesis of NbS_3 whiskers and the dynamic properties of a charge density wave in ultimately thin NbS_3 samples

To begin with, we shall consider the results of NbS_3 (phase II) research [7].

The quasi-one-dimensional NbS_3 compound is known to exist in two phases. Phase I is characterized by high resistance and some semiconducting properties; the crystal lattice is dimerized along the Nb chains. Phase II is remarkable for its CDWs incommensurate at room and higher temperatures; in this compound, CDWs can slide in an electric field. Apart from the high temperature of the Peierls transition (330–370 K), distinctive features of this compound include the strong anisotropy of its properties (as apparent from very weak coupling between the chains) and combination of high-frequency properties with high coherence of CDWs [25–27]. This compound was synthesized earlier by different authors [28], but they had problems with finding phase II whiskers (filamentary crystals), because they were outnumbered by phase I crystals in the material grown. The conditions for reproducible synthesis of phase II crystals have been described in the most recent publications [25–27].

CDW coherence in NbS_3 samples, combined with their high-frequency properties, implies the possibility of high-speed CDW sliding. We reached record-breaking synchronization frequencies with thin NbS_3 whiskers, i.e., extremely high velocities of CDW motion. The maximum current density in most compounds is limited by heating of the samples, while the observation of the generation or synchronization of HF oscillations is hampered by still lower currents. Heating effects can be weakened by selecting the thinnest samples and placing them on a substrate with high heat conduction. However, sample thinning is restricted by the size effect, due to which the threshold voltage V_t initially rises resulting in a decrease in CDW current at the same voltage, and then the CDW state undergoes transition to another dielectric state [16]. It was shown that phase II NbS_3 is an ideal compound for studying synchronization at ultimately high frequencies. Suffice it to say that a CDW retains its characteristic properties at least in samples as thin as 20 nm, due to its marked structural anisotropy. It needs to be emphasized that we conducted most CDW synchronization experiments at room temperature and did not use a cryostat; this facilitated matching the samples and microwave generators.

2.1 Synthesis

The determination of conditions for the reproducible growth of phase II NbS_3 whiskers made possible systematic studies of the properties of this compound, many of which proved unique. Therefore, we start by describing the conditions for phase II NbS_3 synthesis.

Three experiments on NbS_3 synthesis from a gaseous phase at the optimal temperature and its gradient were performed. The whiskers were grown in a three-zone Gero furnace (Germany) with a Modcon temperature control device. The temperature was set separately for each zone and, for instance, the appropriate values were 750, 700, and 650 °C to obtain the distribution shown by the bottom curve in Fig. 1.

An ampule was rinsed with an NaOH solution, then with distilled water, dried in a furnace at 800–900 °C for 48 hours, filled with reactants, and sealed under continuous pumping by a dry pump. The dried ampule was exposed to air for less than one hour. After the ampule was placed in the furnace, the temperature was gradually raised from 200 °C to the desired value at a rate of 20 °C/hr and remained constant thereafter during the entire period of whisker growth (usually 10 days), Variations of the growth period had no influence on the phase I to phase II ratio in finished NbS_3.

The mass of reacting Nb and S components remained unaltered in all experiments. These reactants were utilized in stoichiometric proportion with a small (10%) excess of sulfur on the base of 0.08 g of the end product per cm^3 of the ampule.

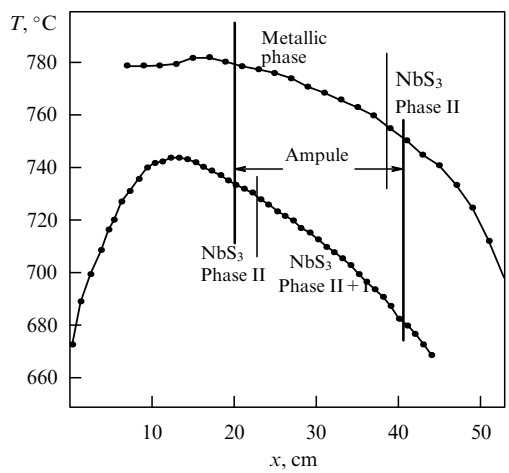

Figure 1. Two variants of temperature distribution over the furnace length (rough measurements in the absence of the ampule). Arrows indicate the positions of the ampule ends. Regions in which each of the two NbS_3 phases grows are shown along with the region where whiskers exhibiting metallic properties grow.

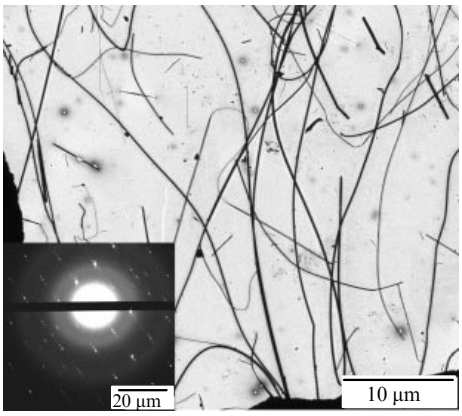

Figure 2. TEM images of NbS_3 whiskers. Inset: an electron diffraction pattern of one of the samples.

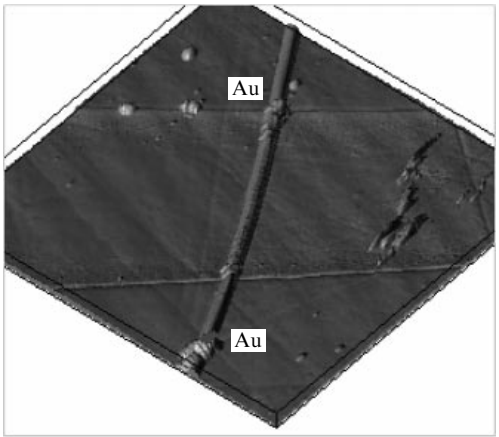

Figure 3. Atomic-force microscopy (AFM) image of an NbS_3 whisker (sample No. 11 from Table 1 in Section 2.4). The scan area is 13.56× 13.56 μm^2. Boundaries of two gold contacts made by the laser deposition method are seen in the image.

The sealing/unsealing procedures, as well as putting the ampule in the furnace, were the same in all experiments.

Two growth cycles were carried out with a temperature gradient of 50 °C for the ampule length (20 cm) (the bottom curve in Fig. 1). The temperature was below 720 °C in one cycle, and above 720 °C in the other. An additional cycle was conducted with a temperature gradient of 25 °C (the top curve in Fig. 1). A few repeated cycles confirmed the reproducibility of the results obtained.

The growth completed, the ampule was opened to remove the 'cocoon' (whisker wool). The transport properties of the whiskers were studied utilizing at least 10 filaments taken at selected points inside the cocoon, viz. at different distances from the cold end of the ampule. It this way, data were gathered on the physical properties of NbS_3 crystals, depending on temperature and its gradient. Figure 1 shows that the optimal temperature for phase II synthesis ranges $\approx 720-750$ °C.

The images of whiskers in a transmission electron microscope (TEM) are presented in Fig. 2; the inset shows the electron diffraction pattern for one of the whiskers at room temperature. Suprastructural reflexes resulting from the creation of two CDWs [26–28] can be seen. Bridge structures (Fig. 3) were made by laser-induced vacuum gold deposition through a micromask.

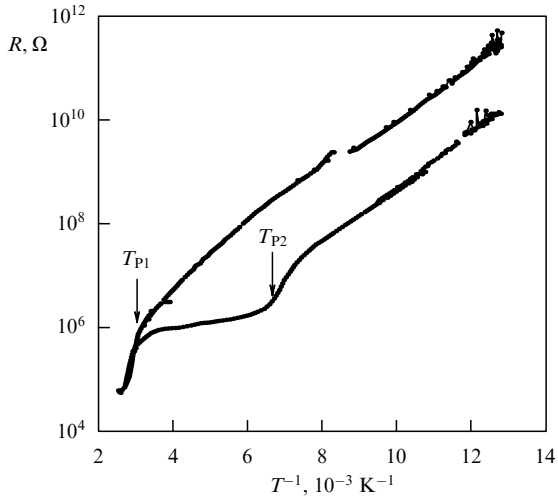

Figure 4. Temperature dependences of resistance for low-resistance (lower curve) and high-resistance (upper curve) NbS_3 whiskers. T_{P1} and T_{P2} are temperatures of Peierls transitions. The samples are 100 μm × 0.13 μm^2 and 90 μm × 0.2 μm^2 in area, respectively. The activation energy for both whiskers is ≈ 1200 K.

2.2 Properties of synthesized samples: nonlinear conduction at room temperature and temperature dependence of conductivity

Detailed measurements of phase II samples permitted distinguishing two groups of them. The samples synthesized at 670–700 °C have lower resistivity; their temperature dependences of resistance, $R(T)$, clearly exhibit two transitions: at $T \approx 360$ K, and $T \approx 150$ K. At synthesis temperatures 715–740 °C, the high-resistance (at room temperature) samples were grown with resistivity by almost an order of magnitude greater; their $R(T)$ dependences had no peculiarities near 150 K, as shown in Fig. 4 presenting characteristic $R(T)$ curves for low- and high-resistance samples. The tendency toward the disappearance of the peculiarity at $T = 150$ K is apparent in thinner samples, too.

The high-resistance samples at room temperature are characterized by a high (up to 80%) degree of CDW synchronization under microwave irradiation (Fig. 5). This suggests a high degree of CDW coherence in the crystal bulk and, therefore, their high quality. Low-resistance samples also exhibited Shapiro steps, but the relative decrease in their differential conductivity (degree of synchronization) was smaller.

At synthesis temperatures below 720 °C and a temperature gradient of 50 °C for 20 cm (bottom curve in Fig. 1), the output of phase 1 (semiconducting) samples shows an outstripping growth rate. Whiskers synthesized at temperatures $T > 760$ °C possess metallic properties (Fig. 6). Their resistivity is at least one order of magnitude lower than that of low-resistance phase II samples. Some dielectrization was observed only at temperatures below 150 K (see Fig. 6), which may be ascribed to 'residues' of the lower transition. There is a well-apparent tendency toward a decrease in lateral sizes of samples with increasing synthesis temperature.

Investigation on the crystals grown was undertaken by transmission electron microscopy at room temperature and confirmed that they fit into phase II samples, as also evidenced by the observation of two Peierls transitions near 365 and 150 K. At the same time, the intersample variation of properties gives evidence of a certain 'hidden' parameter that

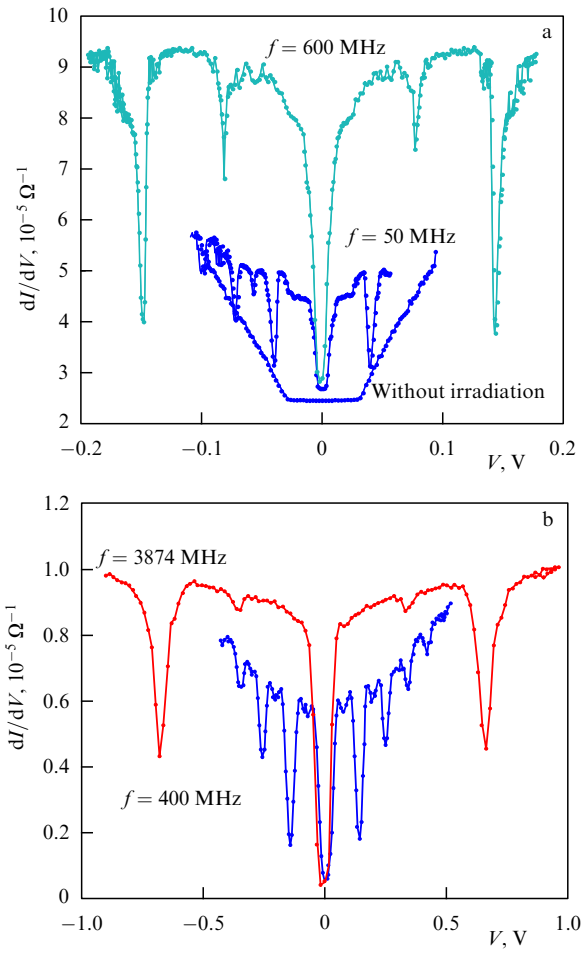

Figure 5. Dependences of differential conductivity of high-resistance NbS_3 samples at room temperature: (a) irradiation at 50 and 600 MHz, and in the absence of irradiation, sample area 7.5 μm $\times(8 \times 10^{-2})$ μm^2; (b) irradiation at 3874 and 400 MHz, sample area 6.5 μm $\times(7.6 \times 10^{-3})$ μm^2.

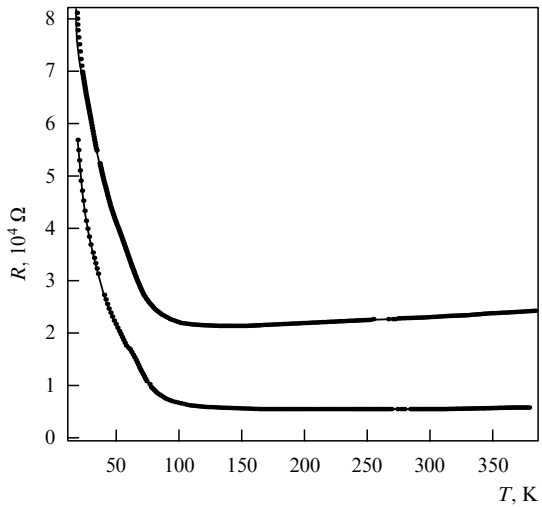

Figure 6. Temperature dependence of resistance for two samples grown at temperatures above 760 °C.

also varies depending on synthesis temperature. For example, a rise in temperature resulted in a marked jump of resistance at the upper transition and its fall at the low-temperature one. In doing so, resistivity at room temperature could show an

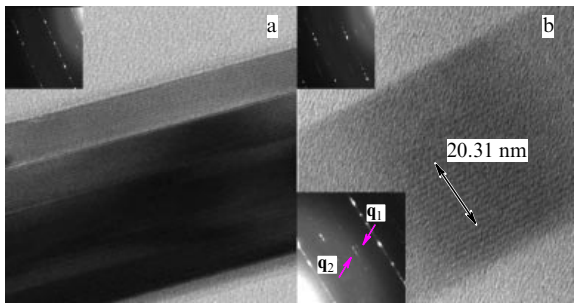

Figure 7. High-resolution electron micrographs of NbS_3 whiskers synthesized at (a) 670–700 °C, atomic layers spaced 9.9 Å apart; (b) 715–740 °C, atomic layers spaced 19.8 Å apart. Scale mark: 10 atomic layers (image scales are identical). Insets: microdiffraction images along direction [001]. Two superstructures are seen: $\mathbf{q}_1 = (1/2a^*, 0.297b^*, 0)$, and $\mathbf{q}_2 = (1/2a^*, 0.353b^*, 0)$.

order of magnitude rise simultaneously with a similar increase in the current–voltage characteristic (CVC) nonlinearity, i.e., a decrease in resistance at high voltages.

The results of structural research suggest that the 'hidden parameter' arises from period doubling along the crystallographic direction a in crystals grown at higher temperatures. Figure 7 presents high-resolution TEM images of samples from different groups. Both images demonstrate the structure of atomic layers extended along the b-axis. In a (low-resistance) sample grown at 670–700 °C (Fig. 7a), the period of this structure along the a-axis equals roughly 10 Å, whereas it is twice that in a (high-resistance) sample grown at 715–740 °C (Fig. 7b). A similar picture emerges from the electron diffraction patterns in the insets to Fig. 7: the period of diffraction pointing along direction a in Fig. 7a is twice that in Fig. 7b, which suggests the formation of a superlattice with the doubling of the period along the a-axis in high-resistance samples.

2.3 Nonlinear conduction at low temperatures

Nonlinear conduction of NbS_3 whiskers was investigated in a wide temperature range. Voltage dependences of differential resistance confirmed the formation of two CDWs in low-resistance samples: there are two temperature ranges in which the dependences take a threshold form [25]. The minimum threshold field E_t is around 2 V cm^{-1} for the upper CDW, and somewhat smaller for the lower one. The highly anisotropic structure of NbS_3 manifests itself in a short CDW coherence length across the chains, as apparent from the weak dependence of E_t on transverse dimensions of samples. Nevertheless, E_t exceeds 100 V cm^{-1} in the thinnest samples, in accordance with the finite-size effect known for other compounds with CDWs [16, 17].

One more peculiarity observed in some phase II samples is worthy of note. It is a sharp increase of resistance in response to a temperature drop in the $T < T_{P2}$ range. This rise may be characterized by an activation energy roughly equal to 2000 K (Fig. 8). Nonlinear conduction at temperatures $T < 150$ K has a threshold form (Fig. 9a) for the majority of the selected samples [25]. However, certain $R_d(V)$ dependences exhibit a sharp peak at $V = 0$ (Fig. 9b). In this case, near-maximum dependences can be roughly described by a power law. Dielectrization upon a drop in temperature and similar $R_d(V)$ dependences were observed earlier for very thin samples of the quasi-one-dimensional

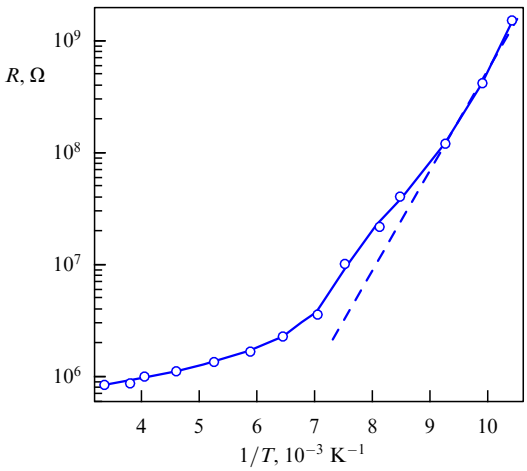

Figure 8. $1/T$ dependence of resistance for NbS_3 samples grown at 670–700 °C. All points are obtained from current–voltage characteristics (CVCs) shown in Fig. 9b. The activation energy at low temperatures is 2000 K (dashed line).

conductor $NbSe_3$ [29]: the peak at $V = 0$ seems to be superimposed on the usual threshold $R_d(V)$ dependence. The authors of Ref. [29] emphasize that such a peculiarity is characteristic of one-dimensional systems, but they failed to unambiguously identify its origin. It should be noted that similar dependences were also observed in $NbSe_3$ samples with artificially introduced defects [30, 31]. Therefore, the most plausible explanation for dielectrization of thin samples reduces to their defective structure. It is also worth mentioning a recent work [32] where power-law (pseudo-power-law, to be precise) dependences $R(V)$ and $R(T)$ in quasi-one-dimensional conductors, including $NbSe_3$, are explained by hopping conduction. This leads to the conclusion that $NbSe_3$ samples with temperature dependences of resistance similar to those presented in Figs 8 and 9b have more structural defects.

We shall turn back to the nature of such CVCs in Section 5, where the compound of a somewhat different type, TiS_3, is considered.

2.4 Limiting currents and synchronization frequencies of a charge density wave

The motion of CDWs in NbS_3 is confirmed by the observation of Shapiro steps (Fig. 5) for both upper and lower CDWs [25]. We prepared samples of the minimally possible small lateral sizes in order to obtain limiting currents (therefore, synchronization frequencies). Cross sections of about 10 such samples were first measured with an atomic force microscope. The study of Shapiro steps in *upper* CDWs of these samples showed that the ratio of CDW current density — corresponding to the main step — to the irradiation frequency was roughly equal for all samples within the scatter of the measurement (i.e., accuracy of cross section measurements) (see Table 1). This means that the cross section area of the samples can be found from the Shapiro steps, i.e., from the ratio of CDW current I_{CDW} to the irradiation frequency [29]. We used this approach in our further work.

The cross section area of the thinnest samples was about 5×10^{-4} μm^2, while the contacts were spaced ≈ 1 μm apart. Shapiro steps were identified in such samples at frequencies higher than 10 GHz. The limiting currents were constrained by the Joule heating of the samples, and limiting frequencies by the microwave power that was possible to feed into them. Better correlation was achieved between short samples and microwave radiation. Figure 10 shows typical $R_d(I)$ dependences at room temperature for the case of microwave irradiation (irradiation frequencies are indicated in the figure). The Shapiro steps, namely R_d maxima corresponding to the most complete synchronization of CDWs, are very apparent on the curves. The dependences of the CDW current

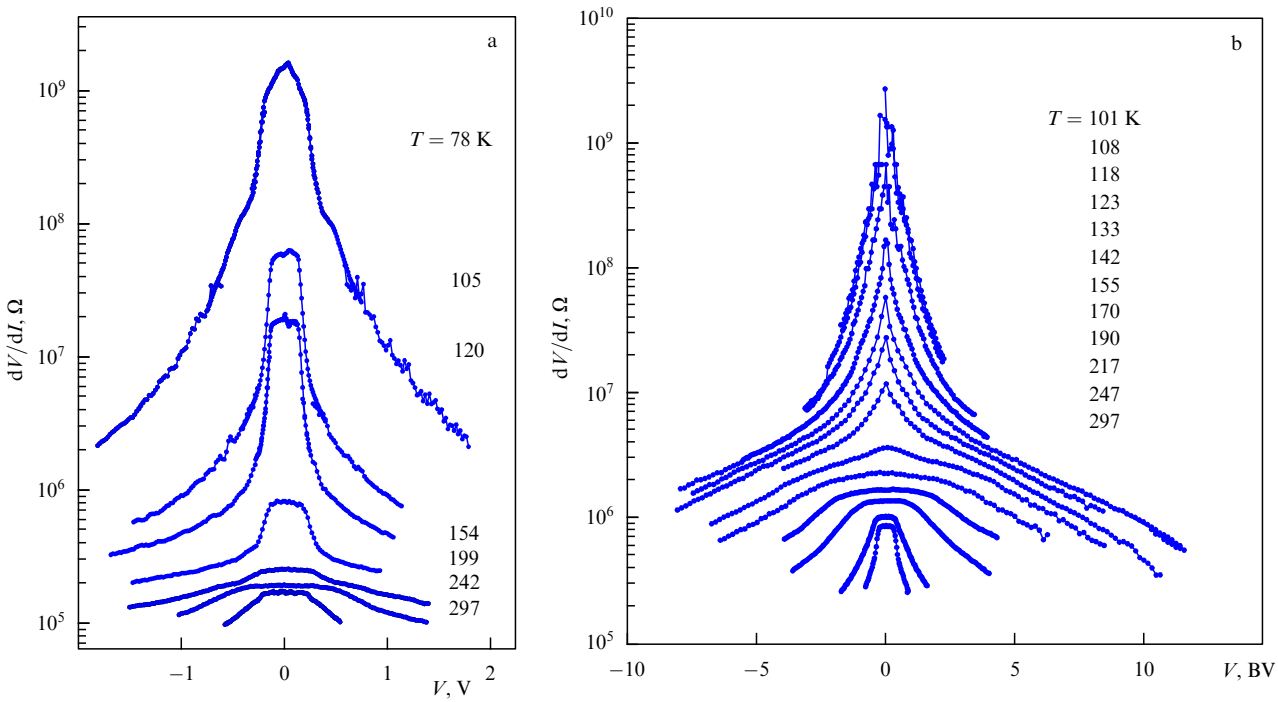

Figure 9. Voltage dependences of differential resistance for two samples grown at $T \approx 715$ °C: (a) low-resistance sample (50 μm × 0.08 μm^2) with two Peierls transitions, and (b) anomalous sample 60 μm ×0.07 μm^2 in size (see Fig. 8).

Table 1. Sample dimensions (width $w \times$ thickness $t \times$ length L) measured by AFM or an optical microscope; temperature T at which synchronization was studied; quantity $I_{CDW}/(2ef_{ex})$, i.e., the number of CDW chains in the sample; area s_0 per CDW chain, and number N of CDW chains per elementary cell, i.e., over an area of 180 Å^2 [7].

Sample	$w \times t \times L$, nm$^2 \times$ μm	T, K	$I_{CDW}/(2ef_{ex})$	s_0, per chain, Å^2	N, per elementary cell
1	140 × 50 × 3.3	295	2.1623×10^3 (< 1 GHz)	322	0.56
2	120 × 50 × 3.7	326	3.84×10^3	156	1.15
3	150 × 20 × 3.2	295	1.95×10^3 1.2806×10^3 (4 GHz)	154 234	1.2 0.78
4	750 × 23 × 3.5	295	10^4	171	1.06
5	160 × 40 × 5.5	295	1875	341	0.54
6	470 × 25 × 42	330 101	2250 1844	522 637	0.35 0.29
7	5000 × 1200	337	2×10^6	300	0.61
8	1000 × 400 × 500	337 131	1.64×10^5 1.05×10^4	244 3.8×10^3	0.75 0.0478
9	90 × 28 × 3	295	1367	184	1
10	44 × 14 × 1	295	304	202	0.9
11	425 × 180 × 7.3	295	3.98×10^4	191	0.94
12	430 × 26 × 8	295	6.585×10^3	169.8	1.06

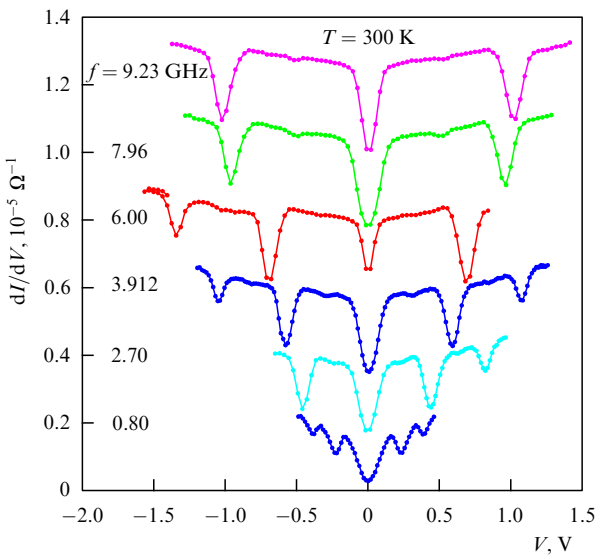

Figure 10. Current dependences of differential resistance for an NbS_3 nanosample 4 μm $\times (1.5 \times 10^{-3})$ μm^2 in size at different irradiation frequencies and room temperature.

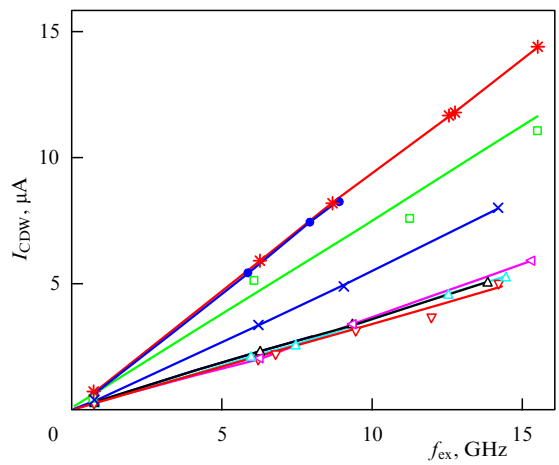

Figure 11. Dependences of CDW current, corresponding to the first Shapiro step, on the irradiation frequency for eight NbS_3 samples at room temperature.

I_{CDW}, i.e., nonlinear current at the main step, on the irradiation frequency f_{ex} are practically linear at frequencies below $f_{ex} = 16$ GHz (Fig. 11).

It is possible to determine the number of chains carrying CDW current (column 4 in Table 1) on the assumption that charge density transferred by a CDW equals $2e$ per chain for a single period, given the known I_{CDW}/f_{ex} ratio. If the sample's cross section area $s = wt$ is measured (column 2), the area s_0 per CDW chain (column 5) is known, too. According to Ref. [7], the area of an elementary cell in NbS_3 is 180 Å^2, with each cell encompassing eight non-equivalent niobium chains. This means that only one of the eight chains in any sample contributes to the upper CDW conduction (i.e., to the Fröhlich mode) (see column 6 in the Table 1).

The 'fundamental ratio' $I_{CDW}/(sf_{ex})$ for the upper CDW is roughly 18 A MHz^{-1} cm^{-2}, or much lower than for the known quasi-one-dimensional compounds. In particular, it is 25 A MHz^{-1} cm^{-2} for both upper and lower CDWs in $NbSe_3$, and 38 A MHz^{-1} cm^{-2} in NbS_3 [33]. The fundamental ratio for the lower CDW in NbS_3 is still smaller [25–27] and varies from sample to sample (see the table). This means that either only part of the elementary cells contribute to CDW conductivity or the charge transferred by the lower CDW is significantly smaller than $2e$ per period. Thus, the nature of the Peierls state at temperatures below 150 K remains unclear to a great extent (see also Ref. [27]).

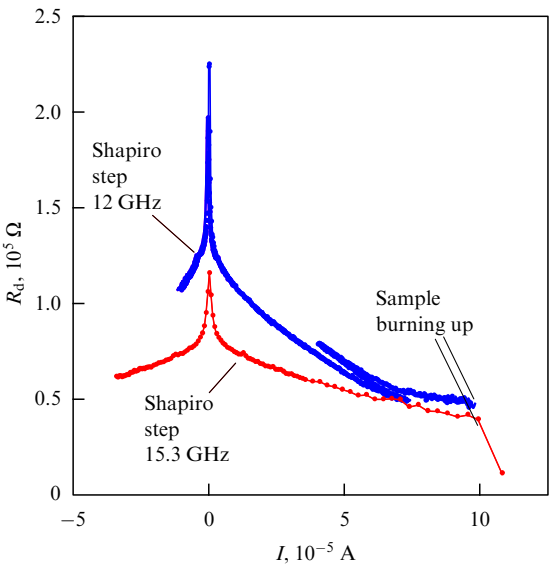

Figure 12. Current dependences of differential resistance for two NbS_3 nanosamples in the case of limiting currents. Sample sizes: 1 μm × (2×10^{-3}) μm^2 (upper curve), and 1 μm × (8.3×10^{-4}) μm^2 (lower curve). The sample undergoes degradation (its resistance grows) in the current range $(5-10) \times 10^{-5}$ A and thereafter burns up.

As far as the upper CDW is concerned, it should be noted that 16 GHz is the highest frequency on record at which CDW synchronization has ever been observed. It corresponds to the sliding CDW velocity on the order of 10 m s^{-1} in the absence of signs of approaching a limiting value associated with either CDW breaking (achievement of critical current) or the loss of its coherence. As mentioned in the Introduction, the indications of achieving the CDW critical current in TaS_3, $NbSe_3$, and blue bronze were reported in Refs [14, 15], but direct evidence of CDW breaking at high sliding velocities is still lacking. According to Refs [14, 15], the critical current corresponds to the fundamental frequency $f_0 \sim 10^{13}$ Hz. Thus far, we have not been able to match nanosamples to microwave radiation in excess of 16 GHz, i.e., feed into them a power sufficient for CDW synchronization. Nevertheless, we have estimated critical currents that can be passed through NbS_3 bridges. To this end, we have measured $R_d(I)$ dependences for a few samples, increasing the current till the sample burnt up or its degradation began (resistance increased).

Figure 12 presents such dependences for two samples. Shapiro steps were observed in them at the limiting irradiation frequencies of 12 and 15.3 GHz (see the corresponding peaks of $R_d(I)$ in the figure). It is seen from these dependences that the maximum current density is $\approx 6 \times 10^6$ A cm^{-2}, the corresponding CDW velocity ≈ 200 m s^{-1}, and the fundamental frequency ≈ 200 GHz. The last value may be regarded as an estimate of the maximum frequency that the samples can receive or generate. These parameters can possibly be enhanced by selecting still thinner samples, i.e., thinner than 10 nm. However, other experimental procedures are needed for this purpose.

The question is, what peculiarities of NbS_3 made it possible to obtain record-breaking CDW synchronization frequencies? Highest current densities on record are due to the aforementioned causes, such as strong structural anisotropy, allowing samples to be thinned to at least 20 nm without suppressing the CDW. Given that such samples fit tightly to the substrate, they can tolerate a current density of up to $\approx 6 \times 10^6$ A cm^{-2} (Fig. 12). Another peculiarity of NbS_3 is the low concentration of conducting chains (one of the eight) responsible for low bulk density of heat release. For a CDW to be synchronized by a microwave field, it must show 'high-frequency properties', besides high sliding velocity. A rigid CDW model and a strongly damped oscillator approximation [34, 35] permit associating such CDW properties of NbS_3 with high threshold fields (≈ 100 V cm^{-1} for nanosamples) and weak CDW friction ($1/\tau$). In this model, the pinning frequency, i.e., the maximum frequency of CDW response to an alternating voltage, is estimated at $E_t e\tau/(\lambda m^*)$ [34, 35].

2.5 Unique properties of charge density waves in NbS_3

A unique property of NbS_3 phase II is the high temperature of transitions. As a matter of fact, the NbS_3 samples grown exhibit three Peierls transitions. TEM studies at room temperature demonstrated the existence of two superlattices (CDWs) with components along the b^* direction: $q_1 = 0.297b^*$, and $q_2 = 0.352b^*$ [28] (the data reported in Ref. [26] agree with those in paper [28]). Satellite reflexes corresponding to q_1 weaken appreciably for $T > T_{P1}$, i.e., starting from temperature 360 K [28]. As the temperature approaches T_{P1}, the threshold nonlinear conduction observed at near-room temperature disappears, too [25], thus meaning that this conduction is due to CDW sliding with q_1. On the other hand, one more CDW remains for $T > T_{P1}$. The study of its properties encounters difficulties because NbS_3 properties begin to degrade rapidly for $T > 400$ K. Nevertheless, fast measurements in the argon atmosphere allowed the temperature of the highest transition, T_{P0}, to be estimated at approximately 620 K. Threshold nonlinear conduction was also observed at temperatures close to 475 K.

The appearance of the third CDW with $T_{P2} = 150$ K is beyond doubt, but the lack of low-temperature diffraction research does not allow us to determine the magnitude of its q vector. Such studies are pending. They are of special interest because charge density carried by the lower CDW appears to be abnormally small and varies from sample to sample.

3. 'Quantization' of charge density wave states in thin samples of blue bronze and $NbSe_3$

Samples of quasi-one-dimensional conductors of submicron and nanometer sizes also possess unique properties in *below*-threshold fields, i.e., when the CDW is at rest. As mentioned in the Introduction, such samples exhibit conduction steps associated with single phase-slip (PS) events, i.e., a change in the number of CDW periods N by ± 1. If contacts create here stringent boundary conditions for the CDW phase, N must be an integer and quantity $q = 2\pi N/L$ must take discrete values. Such 'quantization' of q occurs at the intersection of quantum and classical physics: a CDW comprises a quantum condensate, and its period equals half the de Broglie wavelength of an electron at the Fermi level, $\lambda = \pi/k_F$. At the same time, discrete states of CDWs are similar to the states of a classical wave in a resonator.

In many quasi-one-dimensional conductors, q depends on temperature. Therefore, the CDW period can be altered by changing T. Because the phase slip of CDW requires that a certain energy barrier arising from the necessity of a local CDW break be overcome, $q(T)$ dependences display a hysteretic character (although only indirect evidence of q

hysteresis has so far been available, based on $R(T)$ dependences). This means that states with different q values can be obtained at the same temperature and, vice versa, states with $q = \text{const}$ can be studied in a certain temperature range.

To date, discrete CDW states have not been observable directly, i.e., using electron diffraction methods. (The sole exception is Ref. [19] reporting an X-ray study of thin single-crystal chromium films that yielded discrete q values of spin density waves, depending on the film thickness.) However, the 'quantization' of q is possible to observe, studying T-dependences of σ in micro- and nanosamples. In fields lower than E_t, conductivity is determined by quasiparticles excited over the Peierls gap. Each phase slip changes the charge of CDW and, therefore, the charge of the quasiparticles; moreover, it causes the chemical potential to shift [18]. Thus, jumplike changes of q must be accompanied by σ jumps.

Just such jumps were observed in a study of submicron TaS_3 whiskers [18]. Numerical calculations showed that the magnitude $\delta\sigma$ of jumps corresponds, *on the average*, to the creation and annihilation of a CDW period per chain. Repeated measurements of $\sigma(T)$ confirmed the possibility of observing reproducible discrete states in some cases. However, regular temperature switchovers between the states were never observed. Moreover, the jumps varied in magnitude. There were occasionally much smaller (as if fractional) steps among the majority of roughly equally high ones. Evidently, these deviations from the regular structure of the states are due to incomplete coherence of CDWs both along and across the sample, and to the absence of stringent boundary conditions at the contacts [36].

We conducted a similar study of thin $K_{0.3}MoO_3$ and $NbSe_3$ samples, in which conductivity jumps between discrete states corresponding to 'quantized' values of the wave vector were observed. An important difference from Ref. [18] was the method of contact manufacture, besides the selection and preparation of samples with a perfect structure. The contacts were made by the laser gold deposition technique, ensuring penetration of high-energy gold ions into the material to a depth of several angstroms and induction of radiation defects even farther from the surface. Evidently, such defects sharply enhance the value of E_t and, thereby, prevent the spread of PS-induced CDW strain outside the contact region. This means that the contacts create stringent boundary conditions for CDWs. We also note the low resistivity of such contacts (some 10^{-9} Ω cm^{-2}) and the 'metallic' behavior of their resistivity, suggesting the absence of a contact energy barrier [37].

We selected a few tenths of a micrometer-thick transparent lamellae of blue bronze extended along the b-axis, i.e., along the metal chains. The samples were a few dozen micrometers in length, and several-fold smaller in width [36]. The $NbSe_3$ whiskers were a few tenths of a micrometer in thickness and several dozen micrometers in length. Blue bronze and $NbSe_3$ samples with such dimensions retain the CDW properties characteristic of a bulk material. Detailed results of blue bronze studies are reported in papers [36, 38], and those of $NbSe_3$ in papers [37, 38].

Figure 13 depicts segments of temperature dependences of conductivity $\sigma(T)$ for three samples of blue bronze. The most clear picture of the states and changeover between them was obtained utilizing a $21 \times 5 \times 0.3$-μm^3 sample; it is depicted in the center of the figure showing the hysteresis loop typical of blue bronze. Both branches of the loop exhibit regular temperature jumps of conductivity roughly equal in height.

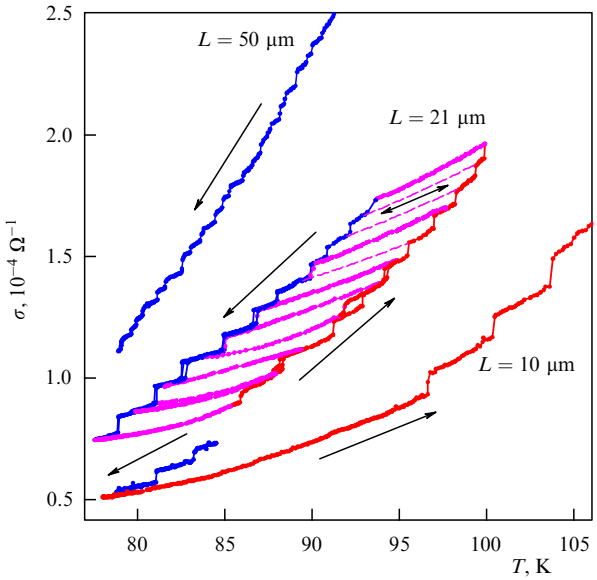

Figure 13. Segments of temperature dependences for three samples of blue bronze. The sample sizes are $21 \times 5 \times 0.3$ μm^3, $50 \times 7 \times 0.3$ μm^3 (conductivity is magnified 1.5 times), and 10 μm × 2 μm (the thickness was not measured, conductivity is divided by 1.5). Arrows indicate temperature scan direction. Dashed lines show omitted reversible segments of the dependence.

The magnitude of the jumps and its changes under the effect of varying temperature are quantitatively described by a semiconductor model. The segments of $\sigma(T)$ connecting the upper and lower branches were obtained by altering the scan direction of T. The $\sigma(T)$ dependences in these curves are reversible, and there are no 'allowed' states between them.

Because each jump corresponds to a $\pm 2\pi/L$ change in q, counting the number of jumps in a certain T range, it is possible to find how the q vector changes within this interval. Specifically, the change in q for $T < 130$ K was observed by this method in Ref. [36]. This observation is consistent with the result of X-ray studies [39], but the responsiveness of q to changes in our case proved much higher ($\delta q/q \sim 10^{-4}$). It was finally found that q continues to change even at temperatures below 70 K. Moreover, a hysteresis of $\delta q(T)$ dependence was revealed.

Because the concentration of electrons or holes (depending on which carriers play the key role) in each chain changes by $\pm 2/L$ in each jump, knowing the $\delta\sigma$ value: the mobility μ of the main carriers can be deduced

$$\mu = \frac{\delta\sigma L^2 s_0}{2es} ,$$

where s_0 is the area per CDW chain, and s is the sample cross section. The value of μ for blue bronze (in the present case, electron mobility) estimated in this way proved to be 10 cm^2 V^{-1} s^{-1}. This value practically coincides with Hall electron mobility of 13 cm^2 V^{-1} s^{-1} [40].

If the mobility is easy to determine in the case of blue bronze by measuring the Hall effect, it is much more difficult to do for semiconductors possessing a more complicated band structure, where different types of carriers make comparable contributions to conductivity. The Peierls' conductors (semimetals) with a complex structure are exemplified by $NbSe_3$. This compound has three types of Nb

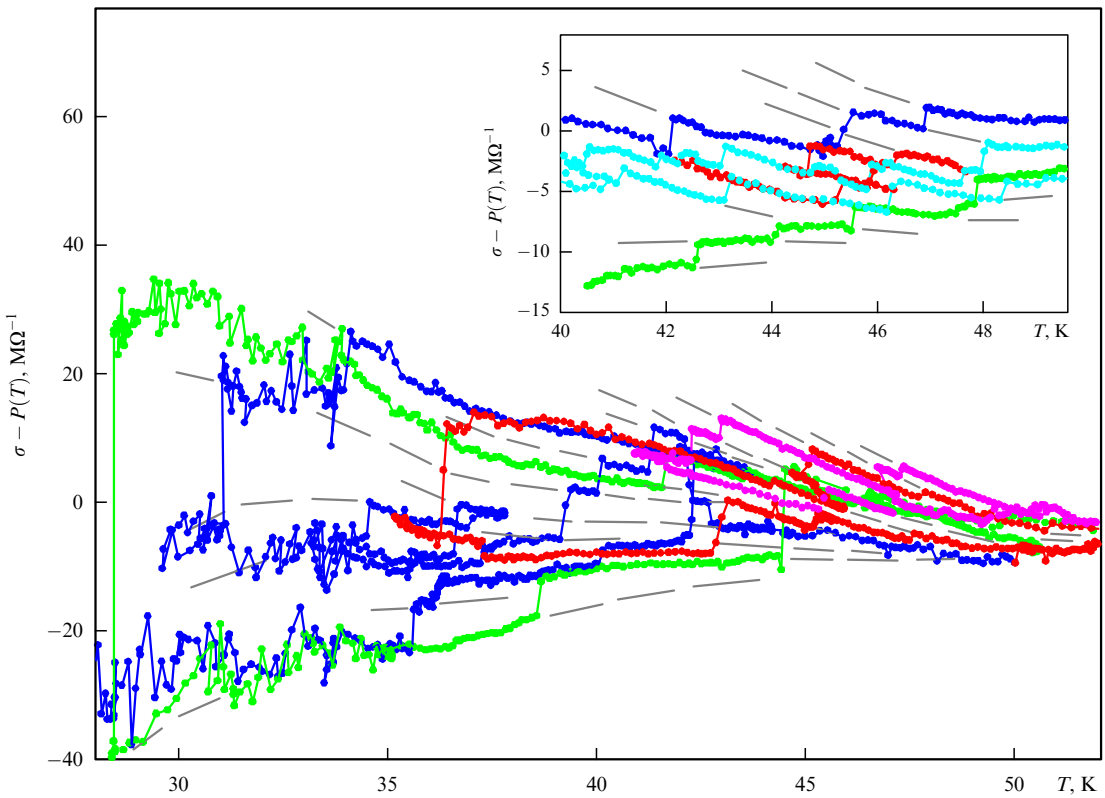

Figure 14. The $\sigma(T)$ dependence obtained after subtraction of polynomial approximation for an $NbSe_3$ sample of length $L = 33$ μm ($R_{300} = 3.2$ kΩ). Dashed lines roughly show omitted reversible fragments of the curves. Inset: a similar dependence for another sample ($L = 35$ μm, $R_{300} = 5.1$ kΩ) in a narrow temperature range.

chains in its structure, each associated with a specific quasiparticle carrier. Investigation of conductivity jumps due to CDW phase slips gives a unique possibility of determining the mobility of exactly those carriers that are associated with a given CDW.

The $NbSe_3$ compound gives evidence of two Peierls transitions: at $T_{P1} = 144$ K, and $T_{P2} = 59$ K. Incomplete dielectrization of the electron spectrum is responsible for a sharp rise in $NbSe_3$ conductivity with decreasing T. Therefore, we approximated the measured $\sigma(T)$ curves for each sample with a polynomial in order to distinguish small changes in conductivity due to single CDW phase-slip events. (The degree of the polynomial varied from 6 to 15.) Then, we subtracted this approximation from the $\sigma(T)$ dependences. The results of this procedure are presented in Fig. 14. The $\sigma(T)$ dependences for $T < T_{P2}$ for two submicron $NbSe_3$ samples were measured during repeated thermocycling. It can be seen from the figure that the curves obtained are actually sets of lines spreading out like a fan with lowering temperature. Each line corresponds to one of the discrete CDW states. The dashed lines help to identify the states that the sample did not occupy during measurements. The observed jumps between the states correspond to single — and sometimes double or triple — phase-slip events.

The most important information to be extracted from the figure is a rise in the magnitude of conductivity jumps $\delta\sigma$ with lowering temperature, which suggests an enhanced mobility of the carriers. The $\delta\sigma$ value was used to determine the temperature dependence of mobility [37]. The results for five samples are presented in Fig. 15. A drop in temperature T to 20 K increased the mobility — it approaches 10^5 cm^2 V^{-1} s^{-1}. It is worth noting that this value was obtained without using

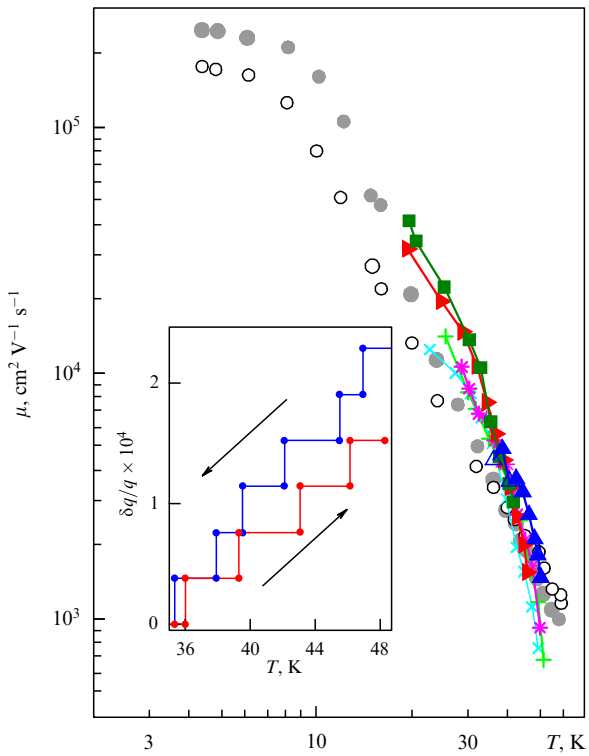

Figure 15. Temperature dependences of mobility obtained by the treatment of $\sigma(T)$ curves for five $NbSe_3$ samples 29–62 μm in length. Unlike symbols correspond to different samples. Full and open dots denote results of model calculation [41] for electron and hole quasiparticles, respectively. Inset: a segment of $q(T)$ dependence for one of the samples (see inset to Fig. 14) obtained on the assumption that each conduction jump corresponds to $\delta q = \pm 2\pi/L$.

any adjustable parameters. Because formation of the lower CDW is believed to be related to the appearance of a gap in the electron spectrum on type 1 chains, it is clear that we found mobilities of quasiparticles connected *precisely with these* chains.

Such a high mobility appears to be due to the presence of 'pockets', i.e., portions of the Fermi surface containing free holes. This unusual property of quasiparticles makes $NbSe_3$ especially interesting for researchers. Earlier authors calculated mobilities of carriers from measurements of the Hall effect, transverse magnetoresistance, and conduction anisotropy with the use of the so-called Ong two-band model. The results of calculation [41] for electrons and holes (principal carriers) are also shown in the inset to Fig. 15. Because six adjustable parameters and certain simplifications were employed in the calculation, its results appear unreliable. Later data suggesting small effective mass of the holes at low temperatures are purely qualitative [42]. Therefore, the rough coincidence between the result thus obtained (Fig. 15) and the results of calculation in Ref. [41] is of importance as the outcome of both the first direct measurement of mobility and the confirmation of the model [41]. Notice that the hole mobility increases even faster than it is expected from the Ong model (open circles in Fig. 15).

Conduction steps also observed in the temperature range $T_{P2} < T < T_{P1}$ are associated with 'quantization' of the states of the upper CDW with $T_P = 140$ K [37]. The mobility of carriers on type 3 chains proved to equal 400–600 $cm^2\,V^{-1}\,s^{-1}$ at $T = 85-135$ K [37], a rather high mobility for quasiparticle excitations of CDW. The steps in this temperature range can be related to the temperature dependence of the q vector of the upper CDW. $q_1(T)$, observed in an earlier study [43]. The $q_2(T)$ dependence has never been reported before for an obvious reason: the change in q_2 over the entire range 20 K $< T < T_{P2}$ is no more than $\sim 10^{-4}$ [37]. Such a change is rather difficult to observe by X-ray techniques.

To conclude, the observation of 'quantization' is not only interesting in itself, but it also allows determining with a high degree of accuracy the mobility of current-carrying quasiparticles. In the case of $NbSe_3$, it also revealed changes in the q-vector value and its hysteresis. The use of 'quantization' of the wave vector values makes it possible to study intricate effects arising from the reorganization of superstructure in different materials and to determine the mobility of carriers in Peierls semiconductors with a complicated structure of conducting bands.

4. Effects associated with deformation of quasi-one-dimensional charge density wave conductors

4.1. Nature of the deformation of quasi-one-dimensional conductors in an electric field

As noted in the Introduction, a CDW can be regarded as an electron crystal formed inside the host lattice and interacting with it. CDW depinning was shown to decrease Young's modulus Y in TaS_3 by 4% [20, 44–47], while the share modulus by the magnitude reaching 30% [20, 48, 49]. These findings were qualitatively explained on the assumption that the deformation of a crystal disturbs CDW equilibrium as well, i.e., results in producing CDW strain [44].

One can also envision the following situation: suppose that a CDW undergoes deformation under the effect of an external force. The interaction of two 'springs', the CDW and the lattice, causes the sizes of the crystal to change in such a way that the CDW approaches equilibrium, and thus the total elastic energy of the CDW and the lattice becomes minimal [22]. Variations of the length of quasi-one-dimensional conductors associated with CDW deformation were observed for the first time under the action of an electric field in Ref. [21]. It was shown that the length of TaS_3 samples may be different, even in a zero field, depending on the previously applied voltage, in connection with residual (metastable) CDW strain. The authors of Ref. [22] reported a change in the length one and a half orders of magnitude greater than in Ref. [21] ($\sim 5 \times 10^{-5}$), with the metastable CDW states in the TaS_3 sample being thermally created. These states are characterized by relatively uniform stretching or compression of the CDW over the sample length.

The semiempirical model proposed in Ref. [52] explains the thermally induced uniform deformation of the samples. Generally speaking, a change in the sample length as a result of CDW deformation can be expected only when the equilibrium CDW period λ nontrivially depends on the lattice parameters. For example, if a change in the lattice period a under the action of an external force alters λ/a, the sample length can be expected to change as a result of CDW deformation. Thus, the TaS_3 strain observed in Ref. [22] is associated with a decrease in the value of a CDW q vector during stretching of the sample, which was revealed in Refs [50, 51]. Model [52] predicts a markedly inhomogeneous longitudinal strain of the sample in an electric field. It is shown that such strain may be L_c/λ times the strain of piezoelectric ion crystals. The ratio of a CDW coherence length to a wave period, L_c/λ, may reach 10^6. However, nonuniform longitudinal strain of quasi-one-dimensional crystals has not yet been observed, presumably due to technical difficulties. An experimental approach with the use of AFM to study such deformation was proposed in Ref. [53].

At the same time, crystal strain need not be longitudinal. Bearing in mind the dependence of λ, not only on longitudinal but also on other components of sample's strain, other forms of inhomogeneous crystal strain in an electric field can be anticipated. Some of them are dealt with in Sections 4.2–4.7.

Torsional strain has been most thoroughly investigated due in part to the availability of relatively simple methods for the measurement of the torsion angle [54–63]. These methods are briefly discussed in Section 4.2.

4.2 Methods of torsion studies

To begin with, a crystal must be fixed so as to enable torsion. With this aim in view one end of the sample 1–5 mm in length and 10–30 μm in width was attached to the substrate by an indium pressure contact so that the sample was elevated above the substrate. The current was fed into the other end through a thin wire — a gold-plated whisker of high-temperature superconductor (HTSC) $Bi_2Sr_2CaCu_2O_x$, which did not really hinder sample twist. Different sample mounting schemes without resort to wires were also used, which is especially important for experiments with the thinnest samples. One scheme took advantage of the relationship between torsion and the presence of a polar axis in the sample that determined twist direction [54]. The sample was cut into halves transversely to conducting chains. One half was turned 180° and the former free end was glued to the cut surface of the other half, giving a structure of two pieces of one sample connected end to end with oppositely directed

polar axes. When the current was passed through this structure, the soldered ends of each piece turned to the same side [62].

Another configuration is much simpler as regards manufacturing technology [58, 62]. Both ends of a whisker were fixed on the substrate by two indium pressure contacts so that its middle part was elevated above the substrate (Fig. 19b in Section 4.5). In this case, half of the suspended part coated with a shunting gold layer served as a passive analog of the tension member, i.e. the wire in the preceding variant. The elasticity of the tension member made, obviously, the torsion angles roughly by half, which was taken into account in the treatment of the results.

In most experiments, torsion was studied by optical methods, in which a laser beam was focused on micromirrors glued to the samples ($Bi_2Sr_2CaCu_2O_x$ whiskers coated with a thin gold layer were also used). An American team studied torsion by a capacitance method based on the measurement of the spiral resonator frequency varying with the movement of the wire glued to the sample [59–61, 63].

4.3 Main results of torsion studies

Here are the main results of torsion research. It was revealed that the free end of the sample in the Peierls state turned as the current was passed through metal chains, with the direction of the turn determined by current direction [54]. Such an effect was observed in a number of CDW conductors: TaS_3, $(TaSe_4)_2I$, $K_{0.3}MoO_3$, and NbS_3 (phase II) [54, 56]. Dependences of the torsion angle on the electric field, $\varphi(E)$, measured at different E variation rates give evidence of two contributions [56]: (1) slow — threshold, hysteretic (see Section 4.4, Fig. 17b, dark curve), and (2) fast — practically linear in terms of voltage. Both contributions are related to CDW strain, probably due to surface pinning. In the first case, the strain was caused by the formation of metastable states; in the second case — by small reversible CDW deformations near an equilibrium or near a metastable state. In the case of 'slow' torsion, shear strain normalized to electric field amounts to 10^{-6} m V^{-1} (at least three orders of magnitude higher than the maximum values of piezomoduli in piezoelectrics). For TaS_3, the time of switchover between metastable strain states after the application of an electric field higher than the threshold one lies in the range $10^{-2}-10^{-1}$ s at liquid-nitrogen temperature and varies approximately as $\exp[900/(T[\mathrm{K}])]$ between 70 and 100 K [56]. Notice that the activation energy equal to 900 K is close to the half-width of the Peierls gap. A somewhat higher activation energy was obtained in Ref. [63], where it is shown that relaxation time decreases with increasing voltage and is invariably higher compared with the known CDW relaxation times found from the dynamics of the electromodulation of TaS_3 reflection index.

The second (fast) contribution [56] is studied less thoroughly. It is smaller than the first one by roughly 1–2 orders of magnitude and prevails in fields below threshold. In this case, CDW strain is small and metastable states do not form; nor does 'slow' strain develop. Moreover, the fast contribution predominates at relatively high frequencies, above 0.1–1 kHz for TaS_3 at $T \approx 80$ K, which distinguishes it from the slow contribution [56]. The upper frequency boundary for such response remains to be found. The TaS_3 torsion amplitude within the limits of experimental accuracy is independent of the alternating current frequency, at least till the first torsional resonance (1–10 kHz) occurs.

The general view of the dependence of torsional response on the amplitude and frequency is given in Fig. 16a [56], where the TaS_3 torsion amplitude is presented as a function of the alternating voltage amplitude in the form of symmetric meander at different alternating voltage frequencies. An analogous set of curves for blue bronze is displayed in Fig. 16b. These dependences suggest that the torsional response at low voltage modulation frequencies shows the threshold dependence on the amplitude. The threshold component of the response decreases with increasing frequency, whereas the linear one barely changes (in TaS_3), or decreases far less significantly (in blue bronze).

The resonant torsional vibrations under the action of an alternating electric field at frequencies up to 200 kHz and Q-factor above 10^4 are associated with 'fast' torsion [57]. In this case, the limiting frequency at which torsion occurs is

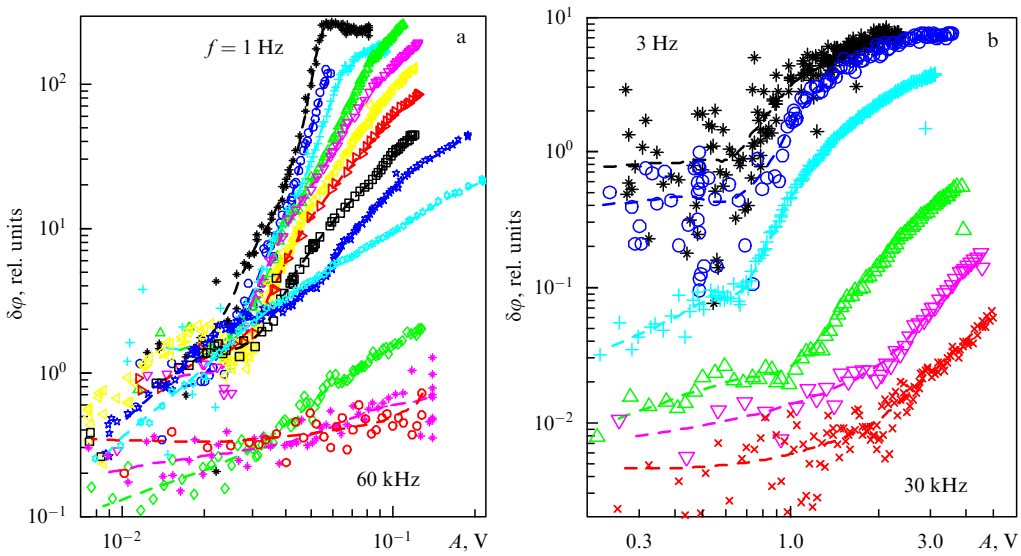

Figure 16. The amplitude of $\delta\varphi$ depending on amplitude A of symmetric rectangular alternating voltage: (a) for TaS_3 at frequencies (from top to bottom) $f = 1, 2, 4, 40, 110, 220, 440, 880, 2\times10^3, 9\times10^3, 15\times10^3, 30\times10^3, 60\times10^3$ Hz, and (b) for blue bronze at frequencies (from top to bottom) $f = 3, 30, 300, 5\times10^3, 10^4, 3\times10^4$ Hz. Dashed curves show smoothed results; the temperature $T \approx 82$ K.

restricted by measuring technique capabilities. The relationship between this contribution and the existence of CDW is well apparent from the behavior of temperature dependence, i.e., a sharp decrease in the amplitude in the Peierls transition region [56].

4.4 Torsional effects associated with the sliding of a charge density wave

The manifestation of CDW strain in the mechanical properties of the samples raised the question about the possible observation of torsional effects associated with CDW sliding, such as synchronization of CDW sliding in an electric field (Shapiro steps) and spatio-temporal nonuniformity of CDW motion apparent as broad- and narrow-band voltage fluctuations at a direct current exceeding the threshold one.

We begin with the Shapiro steps, the finding of which on CVCs suggests increasing *temporal* coherence of CDW motion: a CDW synphasically overcomes the periodic pinning potential at different points of the sample. At the same time, nothing is known about *spatial* coherence of CDW under synchronization conditions, i.e., about the effect of irradiation on the spatially inhomogeneous CDW strain. It is well known that a CDW can slide in a sample continuously without the formation of phase-slip centers in the bulk, as evidenced by the presence of near-contact CDW strain regions extending a few millimeters from the contacts [65]. This extended strain, like inhomogeneous CDW strain developed due to impurities, does not exclude, in principle, the possibility of synchronously overcoming pinning barriers at different points of a sample: the continuity of motion of a CDW means that its phase velocity (hence, fundamental frequency) is identical at all these points. For this reason, even full synchronization of CDW motion during microwave irradiation does not necessarily imply enhanced spatial coherence. Because torsion is associated with spatially inhomogeneous CDW strain, the manifestation of Shapiro steps may provide here information about spatial CDW coherence under synchronization.

Reference [58] reports the results of investigations into the 'slow' torsion of TaS_3 samples during microwave irradiation. Torsional strain was measured simultaneously with $R_d(I)$ dependences that exhibited Shapiro steps, i.e., $R_d(I)$ peaks. The $\varphi(I)$ dependences also showed peculiarities at the same current values at which Shapiro steps were apparent. Direct measurements of $\varphi(I)$ dependences (Fig. 17b, light curve) failed to reveal details of these peculiarities due to low-frequency noises produced by the photodiode and the amplifier. Therefore, we measured $d\varphi/dI$ derivatives depending on I, in analogy with CVC measurement by the synchronous detection method. In so doing, the current modulation frequency proved to be much lower than the frequency of the first torsional resonance (1–10 kHz). The I-dependence of $d\varphi/dI$ exhibited narrow peaks that crossed the $d\varphi/dI = 0$ level (Fig. 17a). This means that under conditions of the fullest CDW synchronization, the sample begins to turn in the opposite direction, as also viewed in Fig. 17b presenting results of direct $\varphi(I)$ measurement (thin curve) together with the results of $d\varphi/dI$ integration. Evidently, the $\varphi(I)$ dependences measured by the two methods roughly coincide, except the hysteretic (slow) contribution, which is practically absent when measured by the differentiation method [58]. The dashed line in Fig. 17b fits approximate results of the $\varphi(I)$ extrapolation in the Shapiro step region in the absence of synchronization. It may be seen that, for the

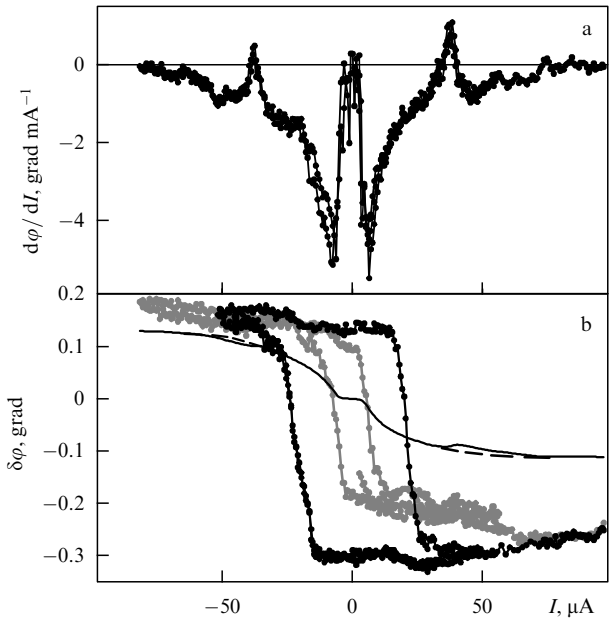

Figure 17. (a) Differential signal from a photodiode (rms value) measured by a synchronous detector during microwave irradiation at 500 kHz. Modulation frequency is 333 Hz (20 times lower than the frequency of first torsional resonance), amplitude $\delta I = 0.6$ μA, and $T = 121$ K. (b) $\varphi(I)$ dependences with (light curve with dots) and without (dark curve) irradiation at 500 kHz. The thin curve is the result of $d\varphi/dI$ integration, and the dashed curve fits approximate results of extrapolation of $\varphi(I)$ in the Shapiro step region in the absence of synchronization [58].

sample being studied, a change in the rotation angle, $10^{-2}\,^{\circ}$, is achieved due to CDW synchronization. The degree of synchronization is estimated at 10% from the $R_d(I)$ dependence [58], which is a good value for TaS_3. Thus, under full synchronization conditions, the torsion angle can be expected to deviate by 0.1° (in fact, zero deviation unless the hysteretic contribution is counted). The decrease in the sample's torsion angle implies that inhomogeneous CDW strain decreases, too, meaning that inhomogeneous CDW strain, at least its torsion-related part (most probably shear strain [54, 56]), must disappear under full synchronization. This finding suggests an enhancement of CDW *spatial* coherence in the presence of Shapiro steps. This conclusion is also consistent with the results of Ref. [66], where Young's modulus maxima and internal friction minima were observed in TaS_3 and $NbSe_3$ samples under synchronization conditions.

As also noted in Ref. [58], torsion measurements can be regarded as a highly sensitive method for studying CDW synchronization. This inference is illustrated by a comparison of peculiarities in the I-dependences of $d\varphi/dI$ and R_d for one of the TaS_3 samples singled out by more chaotic CDW motion. In this sample, the peaks corresponding to Shapiro steps are less pronounced, but peaks corresponding to fundamental frequency harmonics and subharmonics appear. It turned out that the fine structure of harmonics and subharmonics is more apparent in the I-dependence of $d\varphi/dI$ than in the I-dependence of R_d.

4.5 Sample vibrations during the flow of a direct charge density wave current

Shapiro steps research can be regarded as a tool for the study of CDW creep in the periodic pinning potential. This potential is directly manifested as the generation of narrow-

band electric noise during CDW creep. The generation of broad-band low-frequency noise is also associated with pinning and narrow-band noise [67–69]. It can be expected that the motion in the pinning potential must cause inhomogeneous dynamic, i.e., time-dependent, CDW strain.

We present below the results of a study on the dynamic strain of a sample through which direct CDW current is passed. The idea behind this experiment is as follows. If CDW strain results in sample's torsional strain, the dynamic inhomogeneous strain of a sliding CDW is likely to manifest itself as noise (torsional) vibrations (both stochastic and periodic) of the sample.

The first experiments were carried out on samples of $(TaSe_4)_2I$. CDW creep in this compound is distinguished by very low coherence, as apparent from the very indistinct peak of narrow-band noise ($\delta f/f \geqslant 1/10$) [70, 71] and relatively strong broad-band noise. Due to this, the amplitude of stochastic angular oscillations during CDW creep in this compound was higher than in TaS_3. However, difficulties encountered in the preparation of $(TaSe_4)_2I$-based torsional structures, which are related to the fragility of the resulting samples, precluded completion of these experiments. Improvement of the measuring scheme permitted reducing the level of sample vibrations and the amplifier noise; it made possible the study of torsional noises in the TaS_3 samples, as well.

When measuring noise, we ran a direct current I through a sample and recorded, as a rule, the oscillograms of the angle $\varphi(t)$ oscillations with a discretization frequency of 400 Hz for 40 s (16,000 points). Alternating (noise) voltage at the sample was simultaneously recorded in the oscillograph second channel. Discrete Fourier transform was used to find frequency dependences of spectral noise density for angle, $S_\varphi(f)$, and voltage, $S_V(f)$, in a range of 0.025–200 Hz. Measurements repeated at different currents yielded the dependences of spectral noise densities of φ and V on the frequency and current passed through the sample.

A set of $S_\varphi(f)$ dependences for one of the $(TaSe_4)_2I$ samples is presented in Fig. 18. Analogous data for TaS_3 at currents below and above the threshold are shown in Fig. 19b. Figure 19a depicts simultaneously measured dependences for *voltage* fluctuations $S_V(f)$. The following qualitative conclusions are relevant to both quasi-one-dimensional compounds: (1) current passage is accompanied by torsion angle fluctuations in excess of background vibrations (in a zero field); (2) these fluctuations are noticeable only at a voltage close to or above the threshold, and (3) the noise 'turns white', on the average, as V grows: if the difference $S_\varphi(f, V) - S_\varphi(f, 0)$ is approximated by the $1/f^\alpha$ dependence, the exponent α decreases from 2 to 1 for $(TaSe_4)_2I$, and from 1.5 to 0.5 for TaS_3 with increasing V. These observations indicate that vibrations qualitatively reproduce the main features of low-frequency noise associated with CDW sliding [72]. Noise 'whitening' with growing CDW current means that an increase in low-frequency noise precedes that of its high-frequency component. If the noise is regarded in a simplified representation as a result of superposition of two-level fluctuating systems ('fluctuators'), spectral changes related to growing currents suggest a rise in the mean frequency of their switchovers [73, 74].

A detailed comparison of spectral fluctuations of torsion angle and voltage for TaS_3 samples (see Fig. 19) also reveals some differences in their current-dependent evolution. For example, S_V starts to grow gradually even at below-threshold currents, whereas S_φ increases jumplike at a somewhat higher current. In both cases, a further increase in spectral density becomes saturated at currents exceeding roughly two times the threshold value.

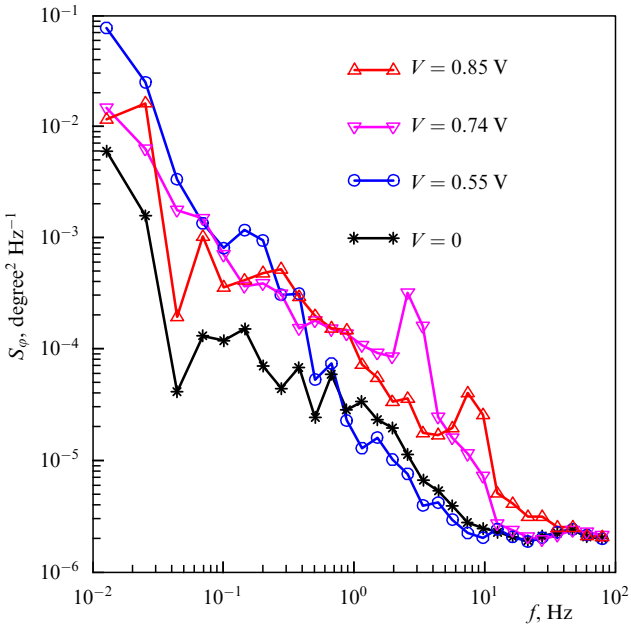

Figure 18. Spectral density of torsion angle fluctuations for a $(TaSe_4)_2I$ whisker during passage of the above-threshold direct current; $T = 147$ K, and discretization frequency is 200 Hz. Fluctuations surpass the noise level ($V = 0$) as the current increases. Threshold voltage is 0.5 V, sample length and width are 1.5 mm and 15 μm, respectively.

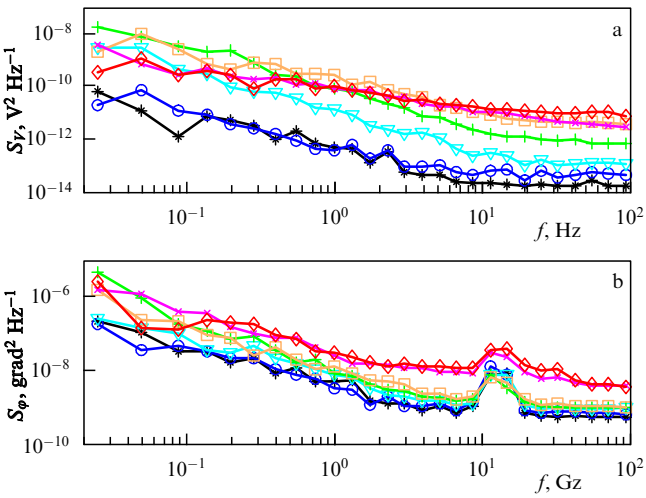

Figure 19. Spectral density of voltage fluctuations (a) and torsion angle fluctuations (b) in a TaS_3 whisker at constant current values 0 (∗), 1.20 μA (○), 2.24 μA (▽), 2.68 μA (+), 2.93 μA (□), 3.17 μA (×), and 3.41 μA (◇). Threshold current is $I_t = 2.8$ μA, length of the gold-free part is 3.5 mm, width 17 μm, and thickness 7 μm; the temperature $T = 83$ K.

Peculiarities in $S_\varphi(f, V)$ curves for $(TaSe_4)_2I$ samples (Fig. 18) need to be studied more thoroughly.

Detailed results of sample's vibration research, including those related to narrow-band noise, are presented in Ref. [75], where it is also shown that the cause of vibrations cannot be reduced to the action of noise voltage associated with CDW creep on the sample: the observed fluctuations of the torsion angle are 2–3 orders of magnitude greater than the angles due to electric noise effects.

Thus, it can be concluded that CDW sliding leads to two independent phenomena: generation of noise voltage, and onset of noise torsional vibrations. In other words, mechanical vibrations are due to the 'direct' mechanical effect of sliding CDWs.

We note that the relationship between torsion angle and voltage fluctuations is not trivial: angle fluctuations depend on inhomogeneous CDW strain, whereas voltage fluctuations may occur without CDW strains, e.g., in a rigid CDW model [13]. We did not find a significant correlation between simultaneously measured $V(t)$ and $\varphi(t)$ oscillograms.

4.6 Nature of torsion

All the main characteristics of torsion allow for the conclusion that it is associated with CDW strain. However, the kind of this strain remains unclear. It was shown in Ref. [54] that torsion cannot be induced by longitudinal CDW strain homogeneous throughout the volume. The relatively small magnitude of the torsion angle temperature hysteresis betokens such a conclusion [54]. The best studied variety of inhomogeneous CDW strain in an electric field, i.e., contraction at one contact and extension at the other, cannot also explain the observed torsion: the torsion angle increases monotonically and almost linearly [54] upon moving off the motionless contact. Therefore, we concluded that the sought-after CDW strain is roughly homogeneous over the sample length but inhomogeneous over its cross section.

It is argued in Refs [54, 56] that such strain may be due to CDW surface pinning and manifests itself in a CDW shear near a surface. As a crystal twists, the largest shear strain develops on the surface. It linearly decreases to zero far from the surface and vanishes at the axis of torsion. Therefore, it can logically be supposed that torsion relates precisely to the CDW strain near the surface. From the symmetry standpoint, torsion may occur in a crystal containing a polar axis. In the case of TaS_3 (rhombic syngony, point group 222 [7]), the polar axis determining torsional direction is absent. In principle, symmetry may be reduced in the Peierls transition, e.g., as a result of transformation of the rectangular cross section of the sample (or elementary cell) into a parallelogram. Such distortion would mean nonequivalence of the adjacent edges of a single-crystal parallel to the conducting chains, and nonequivalence of two directions along the chains. In this situation, 'torsional' surface pinning may occur if the pinning force near the adjacent edges is different.

Torsion may also result from structural defects of a sample. It was shown experimentally in Ref. [54] for three samples cut into halves across the conducting chains that the torsional directions for different pieces coincide if the direction of the chains is preserved. Thus, if torsion is associated with structural defects, such a structure extends over the total sample length. The linkage between structural defects and torsion was confirmed in Ref. [63], showing that the application of an external torque affects the torsion angle and can even cause inversion of the hysteresis loop (Fig. 17a), i.e. a change in the torsional direction at the same voltage sign.

It should be emphasized that the observation of torsion does not mean that a sample is free from developing other comparable strains. One of them, bending, was observed in TEM [56], although the overall strain pattern after the application of an electric field to the sample remains unclear. Specifically, inhomogeneous longitudinal strain expected from the data of Refs [22, 52] needs to be examined (see Section 4.1). Therefore, it cannot be concluded for the moment that shear strain manifested in torsion substantially predominates over other kinds of deformation.

4.7 Voltage modulation induced by torsional strain

Deformation of a sample in an electric field, i.e., an analog of the inverse piezoeffect, raises the question about the possibility of obtaining a signal analogous to the direct piezoeffect, i.e., the electromotive force (emf) resulting from the development of strains. The sample must be a dielectric if emf is to be observed. Resistivity of quasi-one-dimensional conductors at the liquid-nitrogen temperature (torsion is practically unexplored at lower temperatures) as a rule does not exceed $\rho = 1\ \Omega$ cm, which suggests very short charge relaxation time, i.e. Maxwell relaxation time $\tau = \varepsilon\varepsilon_0\rho$, ranging below 10^{-13} s at $\varepsilon = 1$, which excludes observation of the emf caused by developing sample's strain. However, it is worth searching for an analog of the direct piezoeffect at the liquid-helium temperature. The resistivity of TaS_3 samples in these conditions may be on the order of $10^{10}\ \Omega$ cm and higher.

At the same time, torsion (or other deformation) during current passage may produce a feedback signal related to torsion-induced modulation of resistance. Preliminary studies showed that such a signal does exist at above-threshold currents. Reference [57] reports detection of torsional resonances without using optical and capacitance methods. The TaS_3 whisker itself served as the receiver. Alternating current was fed into one part of the sample (actuator) and the signal was detected at another part (receiver) (Fig. 20a). When the alternating current frequency coincided with the resonance frequency, the frequency dependence of the signal had a maximum, suggesting an increase in the torsional vibration amplitude. A similar 'self-sensitive' actuator was designed to have no suspended contact joints (Fig. 20b) [76]. In this case, we modulated the resistance of the motionless part of the sample, contributing to the spread of CDW strain beyond the contact region.

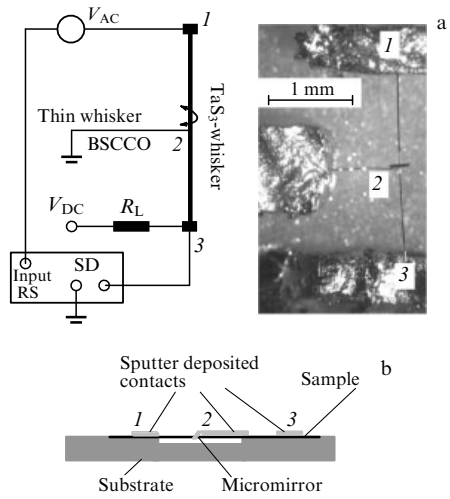

Figure 20. Variants of sample location in detecting resonant torsion without an optical scheme. (a) TaS_3 sample is elevated on two indium contacts [57]. (b) Sample without suspended contact joints: *1–3* — sputter deposited gold contacts [76]. In both cases, alternating voltage V_{AC} exciting vibrations is applied to contacts *1*, *2* and direct current (DC) flows through contacts *3*, *2*. At resonance, a synchronous detector (SD) registers torsional modulation of voltage between contacts *3* and *2*. RS labels reference signal.

The feedback signal was observed only if a direct current substantially higher (roughly an order of magnitude) than the threshold one was passed through the 'receiver'. By a rough estimate, the relative change in voltage in the sample at resonance compares with the surface shear strain of TaS_3: $(\delta V/V)/G \sim 1$. This result means that TaS_3 is not an unusually sensitive strain gauge, at least at liquid-nitrogen temperature.

The tensoelectric response of TaS_3 was more thoroughly investigated in Refs [59, 60], also at liquid-nitrogen temperature. Advantages of the device designed by the authors of Refs [59, 60] included the possibility of exciting torsional vibrations by an alternating magnetic field, although, unfortunately, the capacitance method proved unsuitable for exact calibration of the torsion angle in absolute units (this drawback was corrected in work [63]). It turned out that torsion-induced alternating voltage appeared only when the current was stronger than a certain threshold value in excess of the CDW depinning current. The feedback voltage sharply increased with voltage after this threshold was surpassed. Based on the results of papers [59, 60], the maximum surface shear of the samples was roughly estimated as $G \sim 2 \times 10^{-4}$. Hence, $\delta V/V \sim 10^{-3}$ and the estimate gives $(\delta V/V)/G \sim 5$, close to the above value.

We studied the tensoresistive response of TaS_3 samples at different temperatures. The results are presented below. The idea behind the experiment is that one of the contacts is placed on a motionless substrate, and the other on the bonding pad rotating about the axis roughly coincident with the sample axis, the pad which can be set in motion by a lever extending outward from the cryostat through the rubber gasket sealing and rigidly connected with it. The lever is jointed to the measuring mechanism of an X–Y recorder operating as a torsional actuator. In so doing, the torsion angle of the sample is equivalent to the displacement of the measuring mechanism divided by the lever length (as a rule, of order 1/10 rad). Above-threshold current was passed through the sample, and a 2–20 Hz frequency voltage was applied to the self-recorder. The alternating signal from the sample measured by the lock-in detection method constituted the sought-after tensoresistant or 'torsion-resistant' response.

Figure 21a exemplifies the current dependence of the sample's response. It can be seen that the response emerges at a current above the threshold value of I_t. The shape of this dependence is similar to that obtained in Refs [59, 60], but the signal saturates at currents above $\approx 2I_t$. Moreover, depinning thresholds for CDW (Fig. 21b) and for the appearance of torsional response are not significantly different, unlike those in Refs [59, 60]. At a modulation frequency of 3 Hz, the phase of response is practically unrelated to the current, i.e., the response does not fall behind torsion. It becomes delayed as the frequency increases, i.e., a quadrature signal appears, near the threshold field E_t, and this delay decreases with increasing current. The same conclusion is drawn from Fig. 3 of Refs [59, 60], showing that the quadrature signal at a frequency of 10 Hz first grows with a rise in V and becomes saturated thereafter.

The data presented in Fig. 21a allow the $(\delta V/V)/G$ ratio to be estimated. The value of $\delta V/V$ amounts to 5×10^{-4}, and $G = \delta\varphi\, w/2L \approx 0.07$ rad $\times$ 5 μm/3 mm $\sim 10^{-4}$, which gives the approximated ratio $(\delta V/V)/G \approx 5$, i.e., the same value as in Refs [59, 60]. Similar to the last experiments, the magnitude of the response and its current dependence varied appreciably from sample to sample. Sometimes, the $\delta V(I)$ maximum was

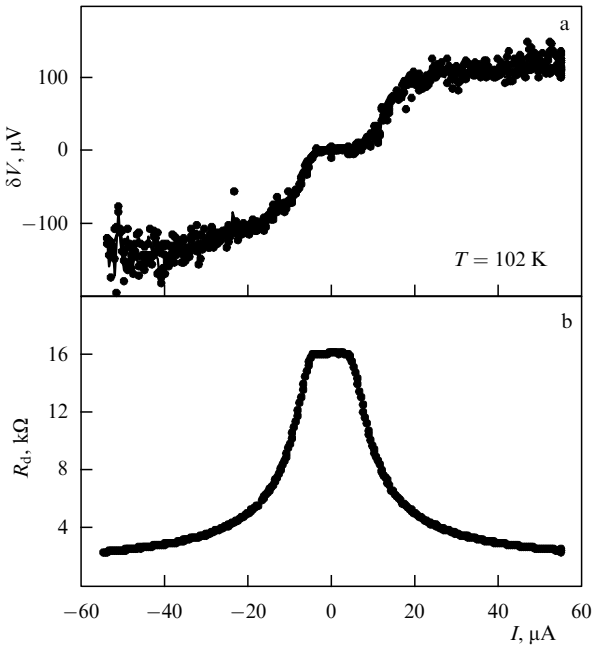

Figure 21. (a) Current-dependent alternating voltage across a TaS_3 sample recorded under torsion angle modulation; $f = 3$ Hz, modulation amplitude is 4°, and sample length 3 mm. (b) Current dependence of differential resistance in the same conditions.

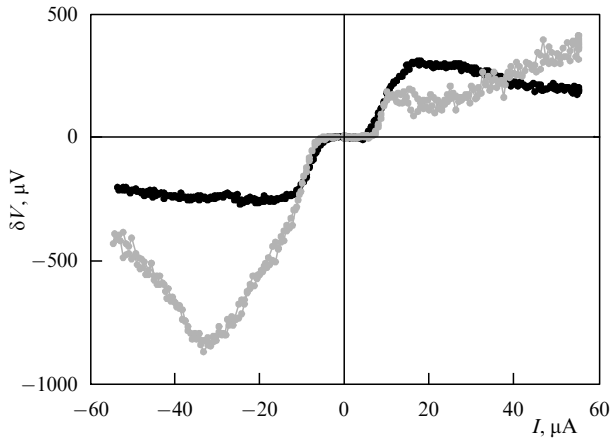

Figure 22. Current-dependent alternating voltage across a TaS_3 sample recorded under torsion angle modulation at $T = 89$ K (dark curve) and $T = 78$ K (light curve); $f = 7$ Hz, modulation amplitude is 3.5°, and sample length 3 mm.

observed instead of saturation (Fig. 22). The character of the dependence changed if a constant torsion angle of ≈ 1 rad ($G \sim 10^{-3}$) was added to the variable $\delta\varphi$.

The dependence was not always symmetric with respect to current reversal. As a rule, a drop in temperature to liquid-nitrogen temperature and below results in a symmetry breaking, as illustrated in Fig. 22 showing $\delta V(I)$ dependences at two temperatures (obtained for the same sample as in Fig. 21 on the next day).

Summarized results of tensoresistance measurements indicate that the $(\delta V/V)/G$ ratio for TaS_3 undergoing torsional strain may reach 5–10. It is a large enough value, bearing in mind that torsion causes only shear strain in which the volume of an elementary cell does not change in the first

approximation. References [77–80] make it possible to estimate (taking into account Young's modulus of 350 GPa [20]) the ratio of $\delta V/V$ to small *longitudinal* strain (tensoresistive coefficient) for TaS_3 as equaling at least 100 in the linear conduction regime (or somewhat below this value in the nonlinear regime). This parameter is comparable with that for p-silicon [81], traditionally employed as a tensoresistive sensor.

Studies into resistive feedback are also of interest from the scientific standpoint, as providing information about the effect of sample's strain on CDW dynamics. At temperatures above liquid-nitrogen temperature, one and the same strain roughly similarly changes the CDW current flowing in different directions. The model proposed in papers [59, 60] describes the modulation of CDW current by varying the threshold field during torsion. The CDW elastic modulus increases at lower temperatures (together with coherence length [82–84]) and the CDW dynamics is described by the motion of large domains. In this case, pinning of individual domains may lead to some asymmetry of the CVC. Accordingly, curves $\delta V(I)$ lose symmetry, too: one and the same torsional strain may have markedly different effects on CDW domains at I and $-I$, because their sizes are comparable to sample dimensions. It remains unclear how the torsional direction is related to the sign of δV. In principle, the relationship between them is feasible in the presence of the helical axis of symmetry that may be inherent in rhombic TaS_3 samples belonging to the point group 222 [7].

5. Nonlinear conduction in the quasi-one-dimensional conductor TiS_3

Sections 2–4 were concerned with group V transition metal trichalcogenides TaS_3, $NbSe_3$, NbS_3, which are typical quasi-one-dimensional conductors with CDWs. In the present section, we report the results of studies of a different sort of quasi-one-dimensional compound, exemplified by TiS_3; we recall that Ti is a group IV transition metal. Most trichalcogenides of such metals ($M^{IV}X_3^{VI}$) belong among diamagnetic semiconductors. Layered quasi-one-dimensional compounds $M^{IV}X_3^{VI}$ crystallize in the monoclinic phase. Metal chains parallel to the *b*-axis make up layers in the *ab* plane separated by double layers of chalcogen atoms. Up to now, the Peierls transition has been documented in the sole representative of this group, $ZrTe_3$. Surprisingly, CDWs originate in *a* and *c* directions perpendicular to the conducting chains [85], rather than along them as usual.

The electron concentration in TiS_3 samples at room temperature measured from the Hall effect [86] reaches $\sim 2 \times 10^{18}$ cm^{-3}, or 3–4 orders of magnitude lower than in known Peierls conductors. This suggests that TiS_3 may be a semiconductor or semimetal. At the same time, titanium trisulfide, like $ZrTe_3$, shows metallic properties at high temperatures: its resistance in the direction along the conducting chains decreases with decreasing temperature. At $T \approx 250$ K, the temperature dependence of resistance $R(T)$ has a minimum. For $T < 250$ K, resistance behaves in a dielectric manner [87, 88] and becomes frequency-dependent [87]. This might be attributed to CDW formation, but no structural phase transition in TiS_3 has thus far been observed [88], and the above result was explained as incidental to disordering. At the same time, nonlinear conduction has recently been reported to occur in TiS_3 at a temperature below 60 K and to increase as temperature continues to drop. Resistance R_d decreased by more than one order of magnitude at $T \approx 4.2$ K in an electric field of ~ 30 V cm^{-1} [80, 90].

Based on CVC measurements along the chains, the authors of Refs [89, 90] argue in favor of a collective mechanism of nonlinear conduction in TiS_3 samples. The dependences $R(T)$ have peculiarities at 120, 59, and 17 K in the form of the maxima of $|\mathrm{d}\ln R/\mathrm{d}T|$ derivatives in *a* and *b* directions, suggesting phase transitions to the condensed state, probably with the induction of a CDW. Temperature dependences of nonlinear conduction (at fixed voltage values) also exhibit peculiarities at the same temperatures as in the case of linear conduction. The growth in TiS_3 conduction anisotropy by two orders of magnitude with decreasing temperature down to $T \approx 50$ K is also a peculiar characteristic of Peierls quasi-one-dimensional conductors [91, 92].

Threshold nonlinearity typical of CDW depinning was also reported in papers [89, 90]. More detailed studies demonstrated the nonlinear behavior of $R_d(I)$ dependence at low currents as well. Conductivity began to increase practically at zero voltage, i.e., the threshold was absent (Fig. 23). As $I \to 0$, an increasingly sharper peak appeared on the $R_d(I)$ dependence as temperature decreased. CVCs had a power-law form at low temperatures (Fig. 24).

As mentioned in Section 2.3, peaks of $R_d(I)$ were observed in certain (seemingly most defective) NbS_3 samples (Fig. 9b), as well as in thin $NbSe_3$ samples with resistance above 1 kΩ μm^{-1} per unit length, i.e., with a cross section area of less than 3×10^{-3} μm^2, and in thick $NbSe_3$ samples with introduced defects [30, 31]. Threshold-free CVCs were also observed in TaS_3 at low temperatures [92].

The heightened interest in such dependences is due to the search for one-dimensional electron states of the Luttinger liquid type [29]. In this case, resistance must show the power-law dependence on temperature and applied voltage. Quasi-

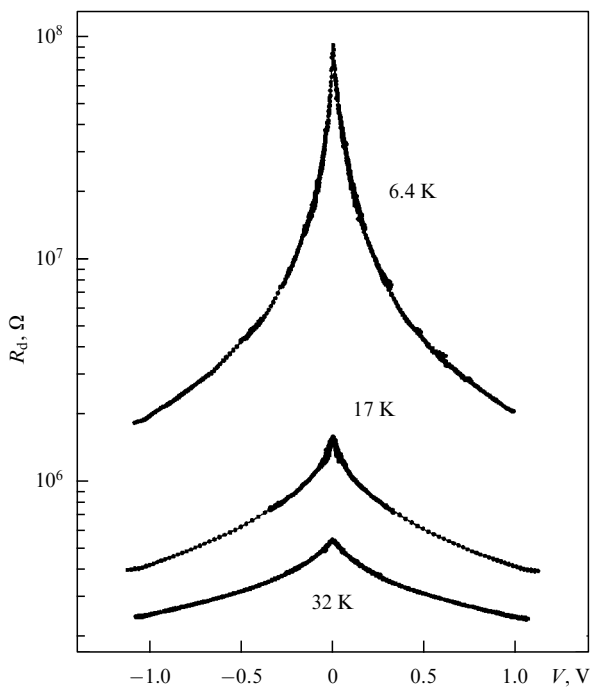

Figure 23. Voltage dependences of longitudinal differential resistance for a TiS_3 whisker at different temperatures. Distance between potential contacts measures 40 μm, and sample cross section area 60×2 μm^2.

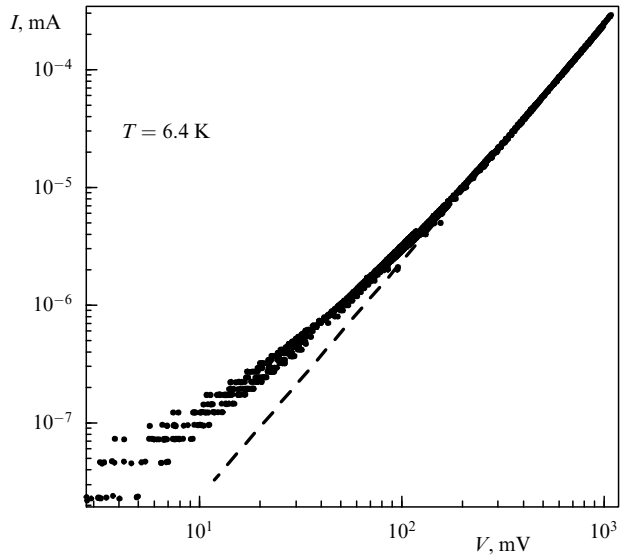

Figure 24. CVC of a TiS_3 whisker measured in the longitudinal direction at T = 6.4 K (corresponds to the upper curve in Fig. 23). For $V > 100$ mV, the dependence has the power-law form: $I \propto V^{\beta+1}$. The slope of the dashed straight line corresponds to exponent $\beta + 1 = 2$.

one-dimensional systems with some degree of disorder may also have an $R_d(I)$ maximum at zero current. Theoretical studies showed [32] that jumplike variations of conductivity in disordered quasi-one-dimensional compounds may be a cause of the power-law dependences of resistance: $R \propto T^{-\alpha}$, and $R \propto V^{-\beta}$. For a Luttinger liquid, one has $\alpha = \beta \approx 2$. In our TiS_3 whiskers, $\beta \approx 1$ near the liquid-helium temperature (Fig. 24). The exponent α found from the slope of $R(T)$ curves in a temperature range $10 < T < 40$ K for different samples proved close to the value of β, namely $\alpha \approx 1.0-1.5$ [93]. In all likelihood, the observed dependences are related to the quasi-one-dimensional character of conduction in combination with electron localization, rather than to the transition to one-dimensional conduction [32]. This reasoning seems especially rational for TiS_3, which shows neither high anisotropy of conduction nor a one-dimensional crystalline structure (crystal lattice parameters are as follows: $a = 0.50$ nm, $b = 0.34$ nm, and $c = 0.88$ nm) [90].

The form of a threshold-free nonlinear CVC in the above cases is determined by the spatially nonuniform potential for carrier motion. The current can be carried here by both one-electron excitations [29–32] and nonuniformly moving CDWs (CDW creep emerges or solitons execute motion) [91, 92, 94]. Nonlinear conduction in TiS_3 occurs for $T < 60$ K and is most likely associated with the phase transition at $T \approx 59$ K, apparent from $R(T)$ dependences [89, 90]. Therefore, it can be supposed that we observe in TiS_3 the nonuniform motion of electrons condensed in a collective state — that is, possibly, a CDW.

Recent studies have shown that the nonlinear conduction in TiS_3 samples also occurs in the transverse direction (along the *a*-axis) at temperatures below 120 K [93]. This nonlinearity appears to be related to CDW formation across the conducting chains in the manner it takes place in $ZrTe_3$ [85].

6. Conclusions

To sum up, the main results discussed in this review were possible to obtain owing to new approaches to the arrangement of experiments, synthesis of compounds (involving new ones) with a perfect structure and coherent CDWs, and application of original methods for preparing micro- and nanostructures based on these materials.

Elucidation of conditions for the synthesis of perfect phase II NbS_3 samples allowed CDW coherent motion to be observed. Synchronization of CDW motion (Shapiro steps) in NbS_3 was observed both at room temperature and T below 150 K. In the former case, a record-breaking 'washboard' frequency of CDWs was obtained with nanometer-thick samples and a CDW synchronization frequency up to 16 GHz. The limiting current density reached in such samples corresponds to the fundamental frequency of 100–200 GHz. Analysis of Shapiro steps gave reason to conclude that at room temperature the CDW current is carried by one of the eight chains contained in an elementary cell. The low density of such chains appears to be a cause behind the possibility of achieving CDW velocities on record in NbS_3 without sample overheating.

Conductivity measurement combined with electron microscopy of NbS_3 samples showed that phase II comprises two groups of samples with different properties determined by growth temperature: whiskers grown at higher temperatures are characterized by enhanced resistance at room temperature and period doubling along the crystallographic *a* direction.

The nature of a lower CDW in NbS_3 ($T < 150$ K) remains to be investigated. The current density carried by this CDW is much lower and strongly depends on sample characteristics. This means that either only part of the elementary cells contribute to CDW conductivity or that the charge carried by a lower CDW is considerably smaller than $2e$ per period. Structural studies of NbS_3 for $T < 150$ K are needed to clarify this issue; they may help to determine the period of CDWs and thereby lay the basis for further work.

In-depth conductivity studies of nanoscale samples of quasi-one-dimensional conductors with CDWs, such as blue bronze and $NbSe_3$, revealed a jumplike variation of resistance (observed earlier in TaS_3 [18]), suggesting specific 'quantization' of the CDW wave vector value. The high coherence of CDWs in these compounds made possible for the first time obtaining a set of discrete states equidistant in terms of conduction. Transition between the neighboring states means a change in the number of CDW periods between the contacts by a unity. Transitions between the states occur as regular temperature-dependent jumps of conductivity. Their temperature distributions were used to derive the temperature dependence of a CDW wave vector $q(T)$; sensitivity to q variations in our case proved substantially higher than that reached by X-ray methods. The mobility of quasiparticles was deduced from the jump magnitudes; it is of special importance for $NbSe_3$ having an intricate band structure. For the first time, we provided direct evidence of anomalously high mobility of residual carriers at low temperatures, suggesting the unique nature of this compound. Thus, q 'quantization' permits us to elucidate some microscopic characteristics of compounds with internal superstructure. In certain cases, this approach has no alternative.

One of the recently emerged lines of investigation into quasi-one-dimensional conductors runs through the research of abnormally large sample strain determined by CDW properties. Of special interest among other kinds of deformation is the huge torsional strain induced by an electric field. Torsion can be regarded as CDW strain transfer to the crystal

lattice, even if neither the form of this strain nor the mechanism of its transfer is known.

It has been shown that torsion contains two contributions: threshold hysteretic and linear. The largest contribution comes from static hysteretic of CDW strain, i.e., strain persisting for the most part after cessation of the application of electric voltage to a sample. At the same time, the dependences $\varphi(I)$ and $\varphi(t)$ exhibit peculiarities that reflect the properties of a sliding CDW. First, HF voltage applied gives rise to peculiarities analogous to Shapiro steps in the $\varphi(I)$ dependences. Their analysis demonstrated enhanced *spatial* coherence of CDWs under synchronization conditions. Second, the flow of a direct CDW current induces torsional vibrations of the samples, reflecting the presence of dynamic CDW strain.

A series of studies was designed to evaluate the influence of TaS_3 twist by an external actuator on the voltage being measured at such samples. No analog of the piezoelectric effect was observed, nor could it be observed owing to the very low resistance of known quasi-one-dimensional conductors with CDWs at temperatures above the liquid-nitrogen temperature. There is every reason to search for an analog of the direct piezoeffect at liquid-helium temperature, when the resistivity of such compounds as TaS_3, $(TaSe_4)_2I$ and $K_{0.3}MoO_3$ is high enough. Torsional strain at temperatures above the liquid-nitrogen temperature results in voltage modulation in TaS_3 samples through which the above-threshold direct current was passed. The maximum relative magnitude of $\delta V/V$ modulation factor normalized to the surface shear ranges 1–10. It is a large enough magnitude, bearing in mind that the volume of an elementary cell during torsion (shear strain) does not change in the linear approximation. This effect is attributed to the action of sample strain on CDW dissipation. For $T \lesssim 90$ K, the $\delta V(I)$ dependence becomes asymmetric, probably due to the rise in CDW coherence volume to a value comparable to the sample volume.

Detailed studies of the transport properties of TiS_3, a still poorly known compound, have been undertaken. It proved to show peculiarities on the temperature dependence of resistance and nonlinear conduction. These findings are explained by phase transitions to the collective electron state. Elucidation of the nature of these transitions (like the transition in NbS_3 at $T \approx 150$ K) is of special interest as occurring in a quasi-one-dimensional compound with a relatively low concentration of electrons. Structure research at low temperatures could elucidate this issue.

Acknowledgments

The authors thank S S Abramchuk for transmission electron microscopy of NbS_3, and R E Thorne and F Levý for the gift of high-quality samples. The work was supported by RFBR (grant No. 08-02-01303-a), the Human Potential Foundation, the Program No. 27 'Fundamentals of Basic Research on Nanotechnologies and Nanomaterials' of the Presidium of the Russian Academy of Sciences, the Program 'New Materials and Structures' of the Russian Academy of Sciences, and the Russian Federation Ministry of Education and Science (Agreement No. 8571). The study was carried out in the framework of the International European Laboratory 'Physical Properties of Coherent Electronic States in Solids' (with the participation of the Kotel'nikov Institute of Radioengineering and Electronics and the Department of Low-Temperature Properties of Solids) supported by CNRS (France), the Russian Academy of Sciences, and RFBR.

References

1. Peierls R *Quantum Theory of Solids* (Oxford: Clarendon Press, 1955) [Translated into Russian (Moscow: IL, 1956)]
2. Fröhlich H *Proc. R. Soc. Lond. A* **223** 296 (1954)
3. Devreese J T, Evrard R P, van Doren V E (Eds) *Highly Conducting One-Dimensional Solids* (New York: Plenum Press, 1979)
4. Fogle W, Perlstein J H *Phys. Rev. B* **6** 1402 (1972)
5. Monceau P et al. *Phys. Rev. Lett.* **37** 602 (1976)
6. Bulaevskii L N *Sov. Phys. Usp.* **18** 131 (1975) [*Usp. Fiz. Nauk* **115** 263 (1975)]
7. Monceau P, in *Electronic Properties of Inorganic Quasi-one-dimensional Compounds* Vol. 2 (Physics and Chemistry of Materials with Low-Dimensional Structures, Ser. B, Ed. P Monceau) (Dordrecht: D. Reidel, 1985) p. 139
8. Grüner G *Density Waves in Solids* (Frontiers in Physics, Vol. 89) (Reading, Mass.: Addison-Wesley Publ. Co., 1994)
9. Brazovskii S, Kirova N, Monceau P (Eds) *Proc. of the Intern. Workshops on Electronic Crystals, ECRYS 2008, Cargèse, France, 24–30 August 2008* (Physica B, Vol. 404, Nos 3–4) (Amsterdam: Elsevier, 2009); *Proc. of the Intern. Workshops on Electronic Crystals, ECRYS 2011, Cargèse, France, 15–27 August 2011* (Physica B, Vol. 407, No. 11) (Amsterdam: Elsevier, 2012)
10. Brazovskii S A, Kirova N N, Monceau P *Physica B* **404** xi (2009)
11. Brazovskii S A, Kirova N N, Monceau P *Physica B* **407** 1683 (2012)
12. Landau L D, Lifshitz E M *Statistical Physics* Vol. 1 (Oxford: Pergamon Press, 1980) [Translated from Russian: *Statisticheskaya Fizika* Pt. 1 (Moscow: Nauka, 1976)]
13. Brown S, Zettl A, in *Charge Density Waves in Solids* (Modern Problems in Condensed Matter Science, Vol. 25, Eds L P Gor'kov, G Grüner) (Amsterdam: Elsevier, 1989) p. 223
14. Sinchenko A A et al. *J. Phys. IV France* **12** Pr9-127 (2002); cond-mat/0101124
15. Sinchenko A A, Thesis for Doct. Phys.-Math. Sci. (Moscow: Moscow Inst. of Physics and Technology, 2010)
16. Zaitsev-Zotov S V *Phys. Usp.* **47** 533 (2004) [*Usp. Fiz. Nauk* **174** 585 (2004)]
17. McCarten J et al. *Phys. Rev. B* **46** 4456 (1992)
18. Borodin D V, Zaitsev-Zotov S V, Nad' F Ya *Sov. Phys. JETP* **66** 793 (1987) [*Zh. Eksp. Teor. Fiz.* **93** 1394 (1987)]
19. Kummamuru R K, Soh Y-A *Nature* **452** 859 (2008)
20. Brill J W, in *Handbook of Elastic Properties of Solids, Liquids, and Gases* (Eds-in-Chief M Levy, H E Bass, R R Stern) Vol. 2 (Ed. M Levy) (San Diego: Academic Press, 2001) p. 143
21. Hoen S et al. *Phys. Rev. B* **46** 1874 (1992)
22. Golovnya A V, Pokrovskii V Ya, Shadrin P M *Phys. Rev. Lett.* **88** 246401 (2002)
23. Weber F et al. *Phys. Rev. Lett.* **107** 107403 (2011)
24. Gor'kov L P *Phys. Rev. B* **85** 165142 (2012)
25. Zybtsev S G, Pokrovskii V Ya, Nasretdinova V F, Zaitsev-Zotov S V *Appl. Phys. Lett.* **94** 152112 (2009)
26. Zybtsev S G, Pokrovskii V Ya, Nasretdinova V F, Zaitsev-Zotov S V, in *VII Konf. 'Sil'no Korrelirovannye Elektronnye Sistemy i Kvantovye Kriticheskie Yavleniya' 18 Iyunya 2009 g., g. Troitsk, Moskovskaya Obl., Tezisy Dokladov* (Proc. VII Conf. 'Strongly Correlated Electron Systems and Quantum Critical Phenomena," June 18, 2009, Troitsk, Moscow region) (Troitsk: Inst. of the High Pressure Physics, Russ. Acad. of Sci., 2009) p. 16
27. Zybtsev S G, Pokrovskii V Ya, Nasretdinova V F, Zaitsev-Zotov S V *Physica B* **407** 1696 (2012)
28. Wang Z Z et al. *Phys. Rev. B* **40** 11589 (1989)
29. Slot E, Holst M A, van der Zant H S J, Zaitsev-Zotov S V *Phys. Rev. Lett.* **93** 176602 (2004)
30. Zaitsev-Zotov S V *Microelectron. Eng.* **69** 549 (2003)
31. Zaitsev-Zotov S V *JETP Lett.* **80** 445 (2004) [*Pis'ma Zh. Eksp. Teor. Fiz.* **80** 503 (2004)]
32. Rodin A S, Fogler M M *Phys. Rev. Lett.* **105** 106801 (2010)
33. Monceau P et al. *Phys. Rev. B* **28** 1646 (1983)
34. Grüner G, Zawadowski A, Chaikin P M *Phys. Rev. Lett.* **46** 511 (1981)
35. Monceau P, Richard J, Renard M *Phys. Rev. B* **25** 931 (1982)
36. Zybtsev S G, Pokrovskii V Ya, Zaitsev-Zotov S V *Nature Commun.* **1** 85 (2010)

37. Zybtsev S G, Pokrovskii V Ya *Phys. Rev. B* **84** 085139 (2011)
38. Zybtsev S G, Pokrovskii V Ya, Zaitsev-Zotov S V *Physica B* **407** 1810 (2012)
39. Girault S et al. *Phys. Rev. B* **38** 7980 (1988)
40. Forró L et al. *Phys. Rev. B* **34** 9047 (1986)
41. Ong N P *Phys. Rev. B* **18** 5272 (1978)
42. Sinchenko A A et al. *J. Phys. Condens. Matter* **21** 435601 (2009)
43. Moudden A H et al. *Phys. Rev. Lett.* **65** 223 (1990)
44. Mozurkewich G *Phys. Rev. B* **42** 11183 (1990)
45. Brill J W, Roark W *Phys. Rev. Lett.* **53** 846 (1984)
46. Jacobsen R L, Mozurkewich G *Phys. Rev. B* **42** 2778 (1990)
47. Xu Z G, Brill J W *Phys. Rev. B* **45** 3953 (1992)
48. Xiang X-D, Brill J W *Phys. Rev. B* **36** 2969 (1987)
49. Rivero A J et al. *Solid State Commun.* **106** 13 (1998)
50. Preobrazhenskii V B, Taldenkov A N, Kal'nova I Yu *JETP Lett.* **40** 944 (1984) [*Pis'ma Zh. Eksp. Teor. Fiz.* **40** 183 (1984)]
51. Preobrazhensky V B, Taldenkov A N, Shabanov S Yu *Solid State Commun.* **54** 399 (1985)
52. Pokrovskii V Ya *JETP Lett.* **86** 260 (2007) [*Pis'ma Zh. Eksp. Teor. Fiz.* **86** 290 (2007)]
53. Pokrovskii V Ya et al., in *Workshop on Recent Developments in Low Dimensional Charge Density Wave Conductors, Skradin, Croatia, June 29 – July 3, 2006*, p. 28
54. Pokrovskii V Ya, Zybtsev S G, Gorlova I G *Phys. Rev. Lett.* **98** 206404 (2007)
55. Gorlova I G, Zybtsev S G, Pokrovskii V Ya "Aktyuator" ("Actuator"), RF Patent No. 2375688. Application 2007141861. Priority of 14.11.2007. Reg. 10.12.2009
56. Pokrovskii V Ya et al. *Physica B* **404** 437 (2009)
57. Pokrovskii V Ya, Zybtsev S G, arXiv:0708.2694
58. Zybtsev S G, Nikitin M V, Pokrovskii V Ya *JETP Lett.* **92** 405 (2010) [*Pis'ma Zh. Eksp. Teor. Fiz.* **92** 448 (2010)]
59. Nichols J et al. *Phys. Rev. B* **79** 241110(R) (2009)
60. Nichols J et al. *Phys. Rev. B* **80** 039903(E) (2009)
61. Nichols J, Sandamali Weerasooriya C, Brill J W *J. Phys. Condens. Matter* **22** 334224 (2010)
62. Pokrovskii V Ya, Thesis for Doct. Phys.-Math. Sci. (Moscow: Kotel'nikov Inst. of Radioengineering and Electronics, Russ. Acad. of Sci., 2009)
63. Zhang H, Nichols J, Brill J W *Phys. Rev. B* **84** 125134 (2011)
64. Rai R C, Brill J W *Phys. Rev. B* **70** 235126 (2004)
65. Itkis M E, Nad' F Ya, Pokrovskii V Ya *JETP* **63** 177 (1986) [*Zh. Eksp. Teor. Fiz.* **90** 307 (1986)]
66. Bourne L C, Sherwin M S, Zettl A *Phys. Rev. Lett.* **56** 1952 (1986)
67. Bhattacharya S et al. *Phys. Rev. Lett.* **54** 2453 (1985)
68. Bhattacharya S et al. *Phys. Rev. Lett.* **59** 1849 (1987)
69. Bloom I, Marley A C, Weissman M B *Phys. Rev. B* **50** 12218 (1994)
70. Wang Z Z et al. *Solid State Commun.* **46** 325 (1983)
71. Mozurkewich G, Maki M, Grüner G *Solid State Commun.* **48** 453 (1983)
72. Bhattacharya S et al. *Phys. Rev. B* **40** 5826(R) (1989)
73. Pokrovskii V Ya, Zaitsev-Zotov S V, Monceau P, Nad' F Ya *J. Phys. IV France* **3** C2-189 (1993)
74. Bloom I, Marley A C, Weissman M B *Phys. Rev. B* **50** 5081 (1994)
75. Nikitin M V, Zybtsev S G, Pokrovskii V Ya *Phys. Rev. B* **86** 045104 (2012)
76. Zybtsev S G, Pokrovskii V Ya, in *INTERMATIC-2008. Materialy Mezhdunarod. Nauchno-Tekhnicheskoi Konf. 'Fundamental'nye Problemy Radioelektronnogo Priborostroeniya', 21 – 23 Oktyabrya 2008 g.* (Proceedings of Intern. Scientific and Technology Conf. 'Fundamental Problems of Radioelectronic Instruments", 21 – 23 October 2008) (Ed. A S Sigov) (Moscow: Energoatomizdat, 2008) p. 18
77. Lear R S et al. *Phys. Rev. B* **29** 5656 (1984)
78. Preobrazhensky V B, Taldenkov A N, Kalnova I Ju, in *Charge Density Waves in Solids. Proc. of the Intern. Conf., Budapest, Hungary, September 3 – 7, 1984* (Lecture Notes in Physics, Vol. 217, Eds G Hutiray, J Sólyom) (Berlin: Springer, 1985) p. 357
79. Preobrazhensky V B, Taldenkov A N *Synthetic Met.* **19** 837 (1987)
80. Das K et al. *Phys. Rev. B* **52** 7915 (1995)
81. Klokova N P *Tenzorezistory* (Resistance Strain Gauges) (Moscow: Mashinostroenie, 1990); Laboratory study "Primenenie tenzorezistorov dlya izmereniya usilii" ("Application of resistance strain gauges for force measurement"), http://www.masters.donntu.edu.ua/2002/kita/gerchikov/lib/lib5.htm
82. Artemenko S N, Volkov A F, Kruglov A N *Fiz. Nizk. Temp.* **14** 356 (1988)
83. Pokrovskii V Ya, Zaitsev-Zotov S V *Synthetic Met.* **32** 321 (1989)
84. Hennion B, Pouget J P, Sato M *Phys. Rev. Lett.* **68** 2374 (1992)
85. Yomo R et al. *Phys. Rev. B* **71** 132508 (2005)
86. Gorochov O et al. *MRS Bull.* **18** 111 (1983)
87. Hsieh P-L, Jackson C M, Grüner G *Solid State Commun.* **46** 505 (1983)
88. Kikkawa S et al. *Phys. Status Solidi A* **61** K55 (1980)
89. Gorlova I G, Pokrovskii V Ya Gorlova I G, Pokrovskii V Ya *JETP Lett.* **90** 295 (2009) [*Pis'ma Zh. Eksp. Teor. Fiz.* **90** 320 (2009)]
90. Gorlova I G, Pokrovskii V Ya, Zybtsev S G *JETP* **111** 298 (2010) [*Zh. Eksp. Teor. Fiz.* **138** 335 (2010)]
91. Takoshima T et al. *Solid State Commun.* **35** 911 (1980)
92. Zhilinskii S K et al.*Sov. Phys. JETP* **58** 211 (1983) [*Zh. Eksp. Teor. Fiz.* **85** 362 (1983)]
93. Gorlova I G et al. *Physica B* **407** 1707 (2012)
94. Nattermann T, Giamarchi T, Le Doussal P *Phys. Rev. Lett.* **91** 056603 (2003)